

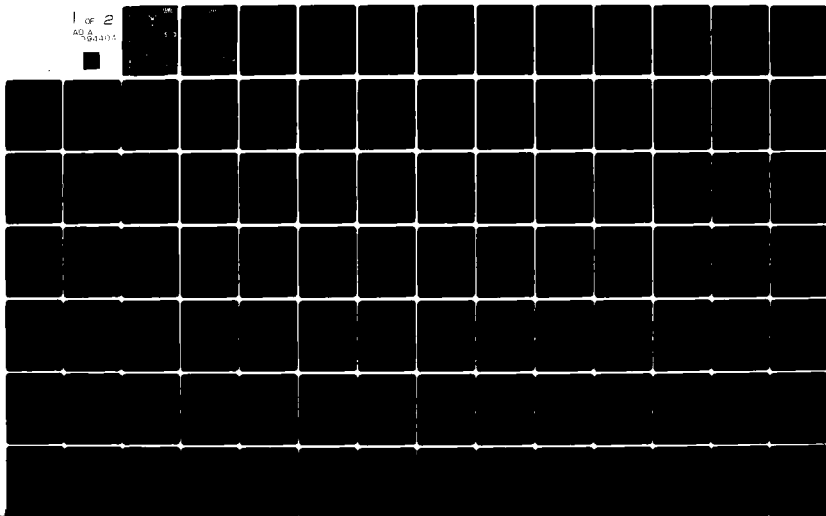
AD-A094 404

AIR FORCE INST OF TECH WRIGHT-PATTERSON AFB OH SCH00--ETC F/G 7/4
MEASUREMENT OF CL2 CONCENTRATION IN A XECL HOLLOW CATHODE DISCH--ETC(U)
DEC 80 J D WINEGARDEN
AFIT/6EP/PH/80-12

UNCLASSIFIED

NL

1 of 2
AD-A094 404

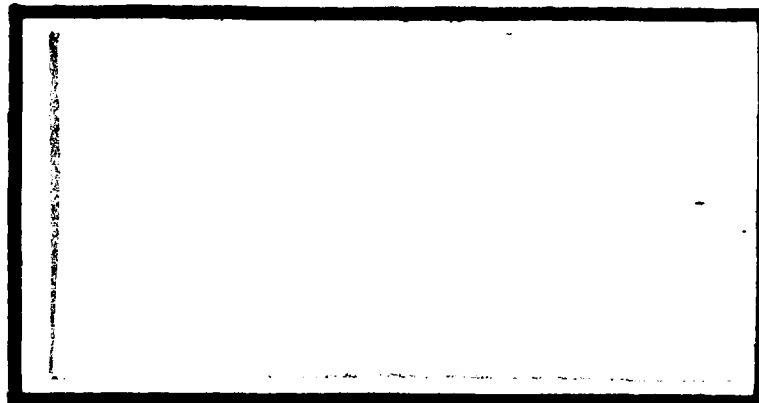


AD A094404



① LEVEL II

DTIC
ELECTE
FEB 2 1981
S B D



DISTRIBUTION STATEMENT A
Approved for public release;
Distribution Unlimited

DEPARTMENT OF THE AIR FORCE
AIR UNIVERSITY (ATC)
AIR FORCE INSTITUTE OF TECHNOLOGY

Wright-Patterson Air Force Base, Ohio

81 2 02 160

FILE COPY

14

AFIT/GEP/PH/80-12

① LEVEL II

14 JAN 1981

APPROVED FOR PUBLIC RELEASE AFR 190-17.

Fredric C. Lynch
FREDRIC C. LYNCH, Major, USAF
Director of Public Affairs
Air Force Institute of Technology (ATC)
Wright-Patterson AFB, OH 45433

⑥

MEASUREMENT OF $C1_2^{17}$ CONCENTRATION IN
A $XeC1$ HOLLOW CATHODE DISCHARGE
INCLUDING THE EFFECT OF H_2^{17} ADDITION.

Master's Thesis

AFIT/GEP/PH
80-12

THESIS

⑩

Jerry D. Winegarden
2nd Lt USAF

Under 291

11 1981

DTIC
ELECTE
S FEB 2 1981 D
B

Approved for public release; distribution unlimited.

412225

AFIT/GEP/PH/80-12

MEASUREMENT OF Cl_2 CONCENTRATION IN A XeCl HOLLOW CATHODE
DISCHARGE INCLUDING THE EFFECT OF H_2 ADDITION

THESIS

Presented to the Faculty of the School of Engineering
of the Air Force Institute of Technology
Air University
in Partial Fulfillment of the
Requirements for the Degree of
Master of Science

by

Jerry D. Winegarden, B.S.

2nd Lt USAF

Graduate Engineering Physics

December 1980

Approved for public release; distribution unlimited.

Preface

The writer wishes to express his thanks to the many fine people who helped in the thesis project. Thanks are given to Dr Peter Bletzinger, Dr Alan Garscadden, and Capt Gary Duke of the Wright Aeronautical Laboratory, Plasma Physics Branch, for contributing their vast resources of knowledge to the project. Thanks also goes out to my advisor, Lt Col W. F. Bailey, for his guidance and suggestions during the project.

A special note of thanks goes to Mr Charles DeJoseph of the Wright Aeronautical Laboratory, Plasma Physics Branch, who led me through the pitfalls of the project and who put up with many inane questions and thoughts by the writer.

Thanks also goes out to Ms Peggy Schram for typing the grading copy of the thesis and to Mrs Anna L. Lloyd for the finalization of it.

Jerry D. Winegarden

Accession For	
ADVISORY	<input checked="checked" type="checkbox"/>
ADVISORY	<input type="checkbox"/>
ADVISORY	<input type="checkbox"/>
Availability Codes	
Dist	Avail and/or Special
A	

Dedication

This thesis is dedicated to my loving wife, Megan, for without her support and concern this thesis would not have been possible.

Table of Contents

	Page
Preface	11
Dedication	111
List of Figures	v
List of Tables	vii
Abstract	viii
I. Introduction	1
II. Theory	11
Kinetics	11
Hollow Cathode Discharge	27
Photon Counting	39
III. Experimental Apparatus and Approach	49
IV. Results	62
V. Conclusions	73
VI. Recommendations	80
Bibliography	81
Appendix A	86
Appendix B	89
Vita	90

List of Figures

<u>Figure</u>		<u>Page</u>
1	Peak Powers of Rare-Gas Halide Lasers under Discharge Excitation	2
2	Potential Energy Curves for a Rare-Gas Monohalide	4
3	Spectral Transmittance of Chlorine	7
4	XeCl* Pulse Output Energy at 308 nm Gas Mixture of Xe/HCl/He:40/4/1950 Torr	8
5	Structure of Rare-Gas Monohalides	12
6	XeCl Potential Energy Curves and Allowed Transitions . .	14
7	XeCl* Emission Spectra from a Hollow Cathode Discharge of a Ne/Xe/HCl Gas Mix	15
8	XeCl* Fluorescence and Laser Spectra under E-beam Excitation	17
9	Characteristics of HCD Used in Thesis Experiment	30
10	Characteristics of a Self-Sustaining Gas Discharge . . .	31
11	Luminous, Electrical and Number Density Variations of a Normal Glow Discharge	32
12	Retarding Voltage vs Collector Current	37
13	Differentiated Retarding Voltage vs Collector	37
14	Low Energy Part of Electron Energy Distribution	38
15	Low Energy Peak vs Pressure x Distance from Cathode; Pressure Ranges of 3-25 Torr and 3.5 mA Discharge Current	38
16	Photon Counting System	40
17	Structure of Photomultiplier Tube	40
18	Spectral Response of Some Photocathodes	42
19	Input and Count Rates for Photomultiplier and Discriminator	47
20	Error Due to Pulse Pile-up for Photomultipliers and Discriminator	47
21	Equipment Arrangement of Thesis Experiment	50

List of Figures (Continued)

<u>Figure</u>		<u>Page</u>
22	Vacuum System and Hollow Cathode Discharge Tube Used in Experiment	51
23	End View of Hollow Cathode Discharge Tube	54
24	Wiring Diagram of PMT Used in Thesis Experiment	56
25	Dark and Light Source Counts Used in Determining PMT Biasing Voltage	56
26	Partial Pressure of Cl ₂ vs Current for a Total Gas Pressure = 4 Torr	66
27	Partial Pressure of Cl ₂ vs Current for a Total Gas Pressure = 6 Torr	66
28	Partial Pressure of Cl ₂ with 0.230 and 0.460 Torr of H ₂ included with a 6 Torr Total Gas Pressure	68
29	XeCl* 308 nm Emission versus Time and Discharge Current at 6 Torr	70
30	XeCl* 308 nm Emission with 0.230 Torr Partial Pressure of H ₂ versus Time and Discharge Current at 6 Torr	71
31	XeCl* 308 nm Emission with 0.460 Torr Partial Pressure of H ₂ versus Time and Discharge Current at 6 Torr	72

List of Tables

<u>Table</u>		<u>Page</u>
I	Comparison of IR and Rare-Gas Halide Lasers	2
II	Some Reaction and Rate Constants for XeCl* Discharges .	28
III	Characteristics of Some Photocathodes	43
IV	Data for 5 Minute Runs Using 3650Å Line	64
V	Variations in Discharge Voltage with and without H ₂ Additions	69
VI	Extinction Coefficients of Cl ₂	87

Abstract

A hollow cathode discharge tube was used to excite a HCl/Xe/Ne gas mixture of 4%/16%/80%. Total gas pressures of 4 and 6 Torr and discharge currents ranging from 200, 300, 400, and 500 mA were investigated. A photon counting technique was used in a U.V. absorption spectroscopy experiment to determine the partial pressure of Cl_2 as a function of current and pressure and for monitoring the 308 nm emission of XeCl^* for these conditions.

XeCl^* emission decreased with time as a result of the introduction of additional chlorine to the system from the discharge tube surface. Both this surface supplied chlorine and that originating from the HCl in the original mix resulted in a substantial concentration of Cl_2 being observed. The surface desorption rate increased with current and was dramatically enhanced by the addition of small amounts of H_2 to the discharge mix.

MEASUREMENT OF Cl_2 CONCENTRATION IN A XeCl HOLLOW CATHODE DISCHARGE INCLUDING THE EFFECT OF H_2 ADDITION

I. Introduction

The properties of the diatomic rare-gas monohalide molecules were essentially unknown as recently as 1974 (Ref 1). Since 1975, rare-gas monohalides such as KrF , XeCl , and ArF have been used extensively as lasing mediums and show such promise that research and development concerning these lasers has grown significantly (Ref 1). Lasers using a rare-gas monohalide as the lasing molecule have demonstrated high output peak and average powers. Peak output powers of greater than 1000 megawatts (1000 MW) have been achieved in some experiments (Ref 2). Commercially available XeCl lasers have peak output powers of up to 25 MW (Ref 2). The output powers attained by these lasers is strongly dependent upon the method of excitation of the laser medium. These methods will be discussed later. Figure 1 shows the peak output powers of the rare-gas monohalide lasers with the laser's corresponding lasing wavelength. The lasing wavelengths are in the ultraviolet (UV) region of the spectrum because the stimulated radiation is from an electronic transition of the rare-gas monohalide. The rare-gas monohalide lasers have also been shown to be fairly efficient. In Table I, the overall efficiencies of some commercially available rare-gas monohalide lasers are shown to be comparable to commercial infrared high power lasers. Having high power and efficient lasers operating in the UV offers some unique applications of the rare-gas monohalide lasers in such areas as laser fusion and underwater communication (Ref 2).

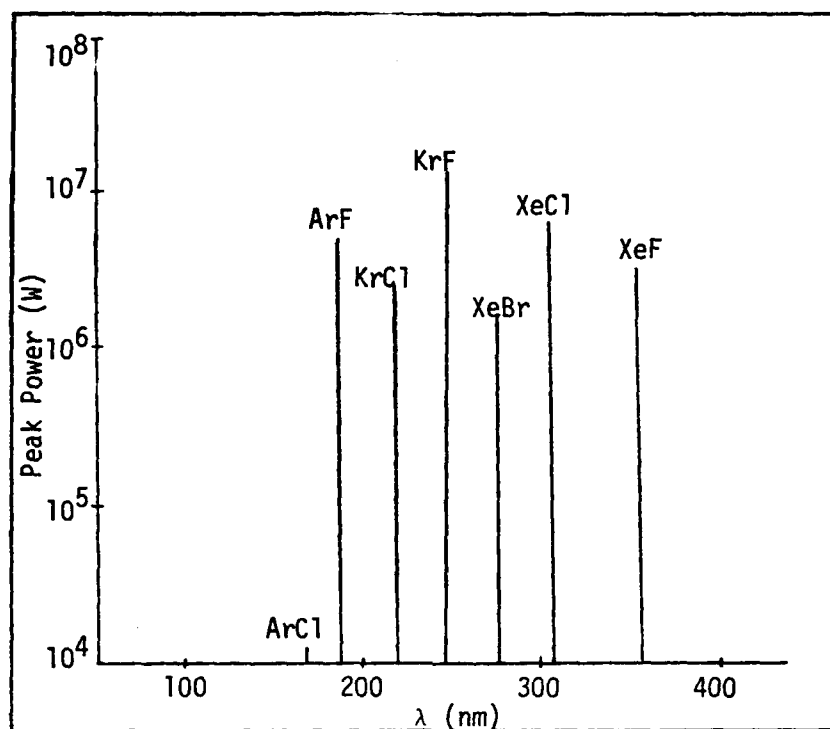


Fig 1. Peak Powers of Rare Gas Monohalide Lasers Under Discharge Excitation (Ref 2)

Table I
Comparison of IR and Rare-Gas Halide Lasers
(Values shown are not necessarily from the same device) (Ref 2)

Spectral Region	Laser	λ , nm	Peak Power MW	Efficiency %
Infrared	CO ₂	10,600	1,000	20
Infrared	Nd:YAG	1,060	10,000	0.1-2
Ultra-violet	KrF	248	25 (discharge)	1-2 (discharge) 7-9 (e-beam)
Ultra-violet	XeCl	308	20-25 (discharge)	1 (discharge) 5 (e-beam)

The rare-gas monohalide lasers typically operate at very high pressures, from 1 to 3 atmospheres. There are various methods of excitation of the lasing medium. One of the methods uses an electron beam (e-beam) for the excitation of the medium, while another utilizes an e-beam in conjunction with a sustainer electric field discharge. Another method of excitation employed is to first preionize the lasing medium with a UV radiation source and then apply a powerful electric discharge. All three of these methods use pulsed excitation, in order to avoid instabilities leading to arcing.

There are several problems associated with the rare-gas monohalide lasers. The halide gases used in such lasers are highly corrosive, causing damage of the discharge tube, electrodes, and optics employed. These gases are also highly electronegative and can cause instabilities in the discharge. The rare gases, such as Xe and Kr, are extremely expensive and are not cost effective when used in a flowing gas laser system. Closed cycle rare-gas monohalide lasers suffer from a degradation in power output as the laser is operated. Development of these lasers and attempts to solve the various problems are currently being pursued. But the question arises, what makes rare-gas monohalides such unique lasing candidates?

The rare-gas monohalides are part of a more general group of chemical species known as excimers. An excimer is a molecule that is unstable in its ground state, but is bound in its excited state. A representative potential energy diagram is shown in Fig 2. The figure shows the repulsive nature of the excimer electronic ground state. The ground state in some excimers may also have a very small well depth associated with it. The dissociation time of the ground state for a

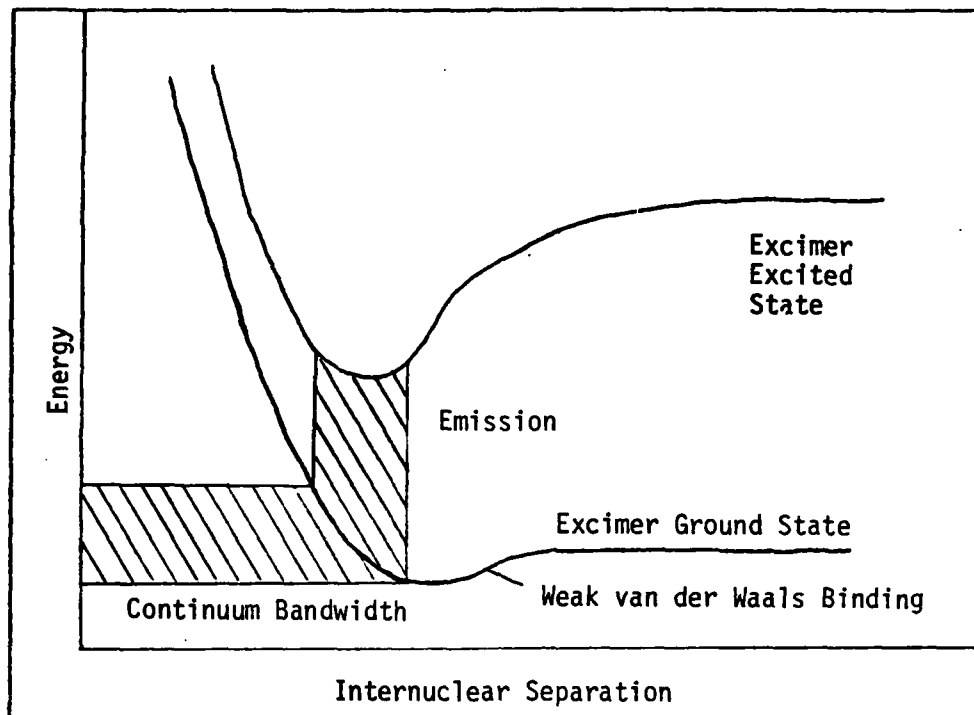


Fig 2. Potential Energy Curves for a Rare-Gas Monohalide
(Ref 1)

rare-gas monohalide is on the order of 10^{-12} seconds. With radiative lifetimes of 10^{-9} to 10^{-6} seconds for the excited state, population inversions between the excited and ground states are easily produced and maintained. The excited state can radiate in a broad band of frequencies, due to the repulsive nature of the ground state. The broad bandwidth of emission from the excited state results in low stimulated emission cross sections for a given frequency of radiation of the electronic transition. The small stimulated emission cross sections give correspondingly low gain for excimer systems (Ref 1). The gain coefficient for a laser medium is given by (Ref 3):

$$\alpha(\omega) = \sigma(\omega) (N_2 - \frac{g_2}{g_1} N_1) \quad (1)$$

where

$\alpha(\omega)$ = gain coefficient as a function of frequency, cm^{-1}

$\sigma(\omega)$ = stimulated emission cross section as a function of frequency, cm^2

N_2, N_1 = number density of upper and lower laser levels respectively, cm^{-3}

$\frac{g_2}{g_1}$ = ratio of the degeneracy of the upper and lower laser levels

From this equation it can be seen that to attain a large gain for lasing, a high population inversion is needed if the $\sigma(\omega)$ is small.

To attain a high population inversion, conditions within the laser should be favorable for excimer formation. The two main reaction channels of formation for the excited rare-gas monohalides are an ion reaction such as (Ref 1):



where M is some third body. The * indicates an excited state. The other reaction involves an excited rare-gas atom reacting with a halogen in a reaction of the type (Ref 1):



Both of these reactions are highly efficient at high pressures. To form the large numbers of rare-gas ions and metastables from electron impact collision requires many high energy electrons. High energy electrons are needed because Eqs (2) and (3) require ionization and electronic excitation, energies much greater than what is needed for

excitation of a laser utilizing a vibrational transition, such as the CO₂ laser. Continuous positive column discharges can not operate at the high pressures required without degenerating into an arc. Electron beams can supply high numbers of electrons at high energies. Some e-beams can deliver a kilojoule of energy in 5 nanoseconds to a gas (Ref 2). Electron beams have been used with sustained electric field discharges also. The e-beam supplies the ionization to maintain the discharge while the sustained field accelerates low energy electrons back up to energies for electronic excitation. UV preionization techniques give the electric field of a discharge a uniformed charge distribution to grow from, deterring instabilities from rapidly occurring. Even these methods are pulsed techniques, due to the high operating pressures and electronegative gases employed.

As mentioned before, the rare-gas monohalide lasers suffer from a degradation in laser output power with time if the laser is operated in a closed cycle fashion. The XeCl laser system, one of the most powerful and efficient of the rare-gas monohalide lasers, has received a great deal of interest due to its long life operation. The lifetime of a laser is generally defined as the time (or number of pulses) it takes until the laser's output power is one-half of the initial output power. XeCl lasers have demonstrated the longest life time operations of the rare-gas monohalide lasers with as many as a million pulses being achieved. A XeCl laser medium consists of a buffer gas of a light rare gas such as He or Ne, the rare gas Xe, and a halogen donor species, such as Cl₂ or HCl. A severe lack of knowledge about the reactions within a XeCl discharge has severely hampered attempts to explain the power degradation associated with the laser.

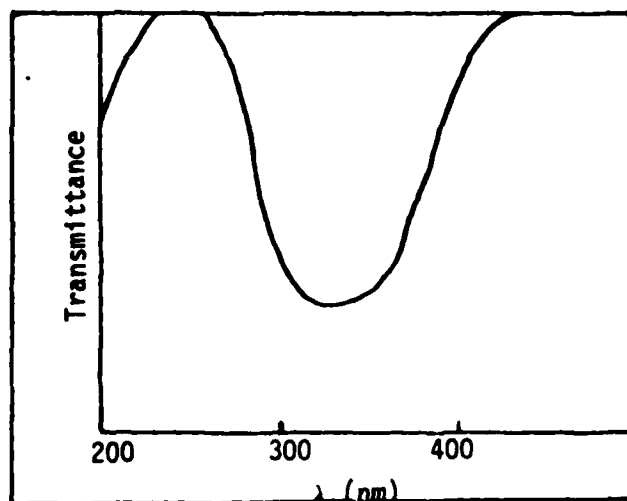


Fig 3. Special Transmittance
of Chlorine (Ref 4)

A proposed explanation for the cause of the power decline is that there is a buildup of Cl_2 within the discharge. Since Cl_2 is a strong absorber in the UV (see Fig 3), an increase in Cl_2 in the laser medium will increase the amount of Cl_2 absorption of the 308 nanometer (nm) lasing radiation, causing the output power to decline. The explanation is aided by the fact that XeCl lasers using HCl as the halogen donor have demonstrated higher efficiencies than XeCl lasers using Cl_2 (Ref 5). An experiment conducted by McKee (Ref 6) found that by adding small amounts of H_2 to a laser medium of He/Xe/HCl, the laser output pulse energy was fairly stable and the lifetime of the laser was extended (see Fig 4). The operating parameters were 1994 Torr total gas pressure and a pulsed discharge. The rationale for adding the H_2 was to force the reaction:



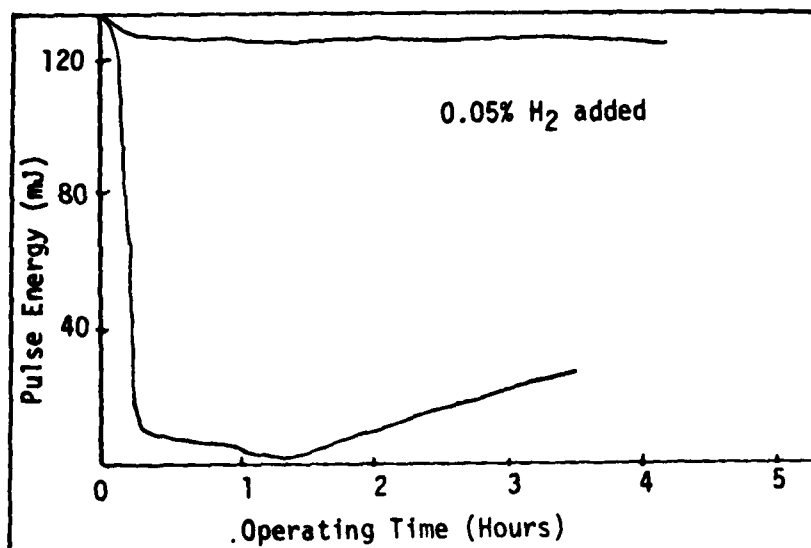


Fig 4. XeCl* - Pulse Output Energy at 308 nm
Gas Mixture of Xe/HCl/He: 40/4/1950 Torr
(Ref 6)

to the left, increasing the HCl concentration and decreasing the Cl₂ concentration.

The purpose of this experiment was to investigate rare-gas mono-halide excimer kinetics and chemistry at low pressures in a HCD geometry. Specifically, the measurement of the concentration of Cl₂ with varying total gas pressures and currents in the discharge was conducted. The effect of the addition of H₂ into the discharge on the Cl₂ concentration and XeCl* emission was also observed in the experiment.

To determine the Cl₂ concentration within the discharge, a UV absorption spectroscopy technique was used (as noted before, Cl₂ is a strong UV absorber). A mercury discharge lamp was used to supply the UV radiation. The gas mixture used throughout the experiment was a Ne/Xe/HCl mix of 80%/16%/4% respectively. The mix composition was decided upon after looking at XeCl* spectra from a discharge within the

hollow cathode taken previously by George Vogel (Ref 7). This mixture was found to give the most intense XeCl* emission. The intensity of the UV radiation was monitored by photon counters, after the radiation has been passed through a monochromator. The absorption of the radiation by Cl₂ follows Beer's Law:

$$I = I_0 e^{-n\sigma x} \quad (5)$$

where

I = the radiation intensity after passage through the gas

I_0 = radiation intensity

n = number density of absorbing species, cm⁻³

σ = cross section for radiation absorption by the species, cm²

x = distance radiation traveled through the gas, cm

To be able to understand and analyze the results of the experiment as presented in Chapter four, one must understand the various attributes of the experiment. The kinetics of the laser discharge, i.e., the possible ionizations, excitations, rare-gas halide formations and quenching, need to be understood if any reasonable explanation of the results can be proposed. The limitation or favoring of any kinetic processes due to the hollow cathode discharge need also be examined. Therefore, the physics of a hollow cathode discharge need to be known. The limitations and errors introduced by the measuring technique need to be examined. Therefore, photon counting techniques have to be understood. The theory of the laser kinetics, hollow cathode discharge, and photon counting are presented in Chapter two. The experimental apparatus and measurement procedure are outlaid in Chapter three.

The conclusions drawn from the experimental results are presented in Chapter five. Recommendations for future work to strengthen or verify our conclusions are presented in Chapter six.

II. Theory

Excimer lasers have been extensively studied with most of the research being in rare-gas halide lasers, due to the high efficiencies and high average power outputs demonstrated by these lasers. XeCl lasers have received special interest due to their long life operation relative to other rare-gas monohalide lasers, as well as XeCl's high power and efficiency. Much is known about the XeCl molecule itself, but the laser reaction kinetics are not completely understood. Involved in the reaction kinetics of the XeCl laser plasma is the formation of Cl₂, which absorbs the XeCl* laser emission (308 nm). The purpose of the experiment was to measure the Cl₂ partial pressures with varying current, total pressure, and H₂ concentrations in a hollow cathode discharge.

Kinetics

Due to the complexity of excimers (He₂^{*}, one of the simplest excimers, has over sixty electronic states (Refs 8 and 9)), the discussion of the energy levels of excimers will be limited to the levels involved only in the lasing transitions. The reaction kinetics involved in the formation of XeCl* are not yet completely understood. Unless otherwise referenced, material for this section was taken from "Rare Gas Halogen Excimers", Topics in Applied Physics, Volume 30, Chapter 4, written by Ch. A. Brau and edited by Ch. K. Rhodes, Berlin and Heidelberg: Springer-Verlag, 1979.

A typical potential energy diagram of the laser levels for a rare-gas monohalide is shown in Fig 5. The lower laser level of a rare-gas monohalide, such as XeCl, is its covalently bonded ground

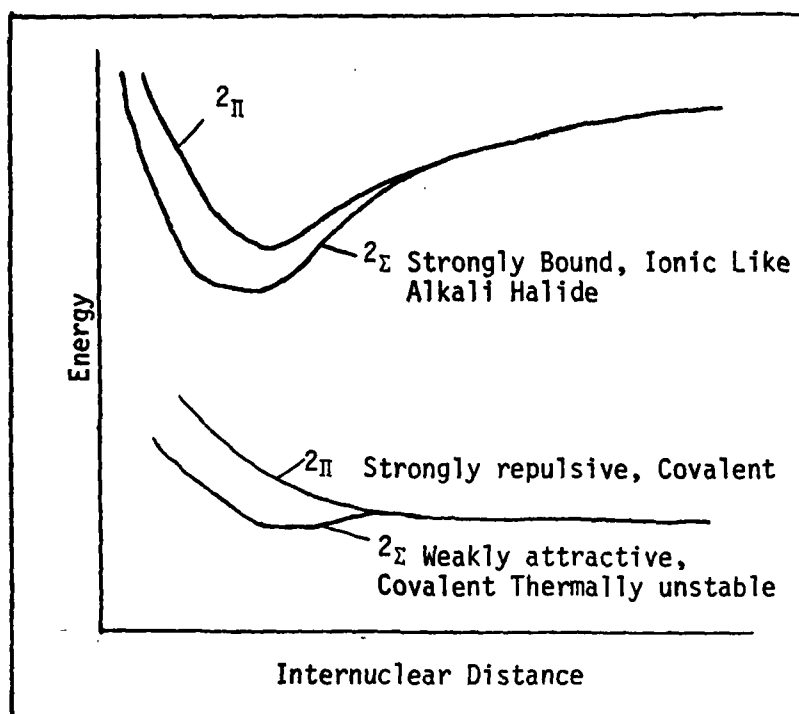


Fig 5. Structure of Rare-Gas Monohalides

state. The ground state is derived from a $1S$ ground state rare-gas atom and a $2P$ ground state halide atom. The net orbital angular momentum of 1 of the P state of the halogen results in the ground state being split into two states, 2Π and 2Σ . When spin-orbit interactions are taken into account, the 2Π state splits into the $2\Pi_{1/2}$ and $2\Pi_{3/2}$ states. By convention, the 2Σ state is referred to as the X state and both 2Π states are collectively called the A state.

The upper laser level is an ionically bound charge transfer state. The level is derived from a $2P$ rare-gas positive ion and a $1S$ halogen negative ion. Just as the ground state manifold was derived from atoms having states of $1S$ and $2P$ orbital angular momentum, so is the upper laser level. As can be seen from Fig 5, the upper level splits at

close internuclear separation. In rare-gas halides in general, the lowest state in the upper level manifold is the $^2\Sigma$ state, referred to as the B state. The upper state of the manifold is a $^2\Pi$ state, which when spin-orbit coupling is taken into account, splits into total axial angular momentum states of $\Omega = \frac{1}{2}$ and $\Omega = \frac{3}{2}$. These states are referred to as the D and C states respectively.

The potential energy curves for the upper and lower laser levels of XeCl as calculated by Hay and Dunning (Ref 10) are shown in Fig 6 along with the allowed electric dipole transitions. However, Brashears and Setser (Ref 11) have conducted recent experiments that indicate that the C state is below the B state of XeCl by 230 cm^{-1} . A possible explanation for this is that in the $^2\Sigma$ state, a singly occupied orbital of one atom is so close to an orbital of the other atom that the interaction or charge transfer between the two atoms may take place more easily than in the $^2\Pi$ state, where the singly occupied orbital is perpendicular to the molecular axis and distant from the other atom (Ref 12). The X state of XeCl has a potential well depth of 255 cm^{-1} (Ref 13).

Figure 7 shows a spontaneous emission spectra of XeCl* from a hollow cathode discharge utilizing a mixture of HCl and Xe with a Ne buffer at 4 Torr total pressure and a total current of 200 mA. The mix was of the ratio 80%/16%/4% of Ne/Xe/HCl (Ref 7). The $(B, \frac{1}{2} \rightarrow X, \frac{1}{2})$ transitions occur from 210 to 312 nm (Ref 14). This is the strongest transition band for XeCl because the initial and final orbitals which the electron resides in have the largest overlap of any of the valence orbitals (Refs 15, 16, and 17). The $(C, \frac{3}{2} \rightarrow A, \frac{3}{2})$ and $(D, \frac{1}{2} \rightarrow A, \frac{1}{2})$ transitions occur from 312 to 460 nm (Ref 14). The broad band of

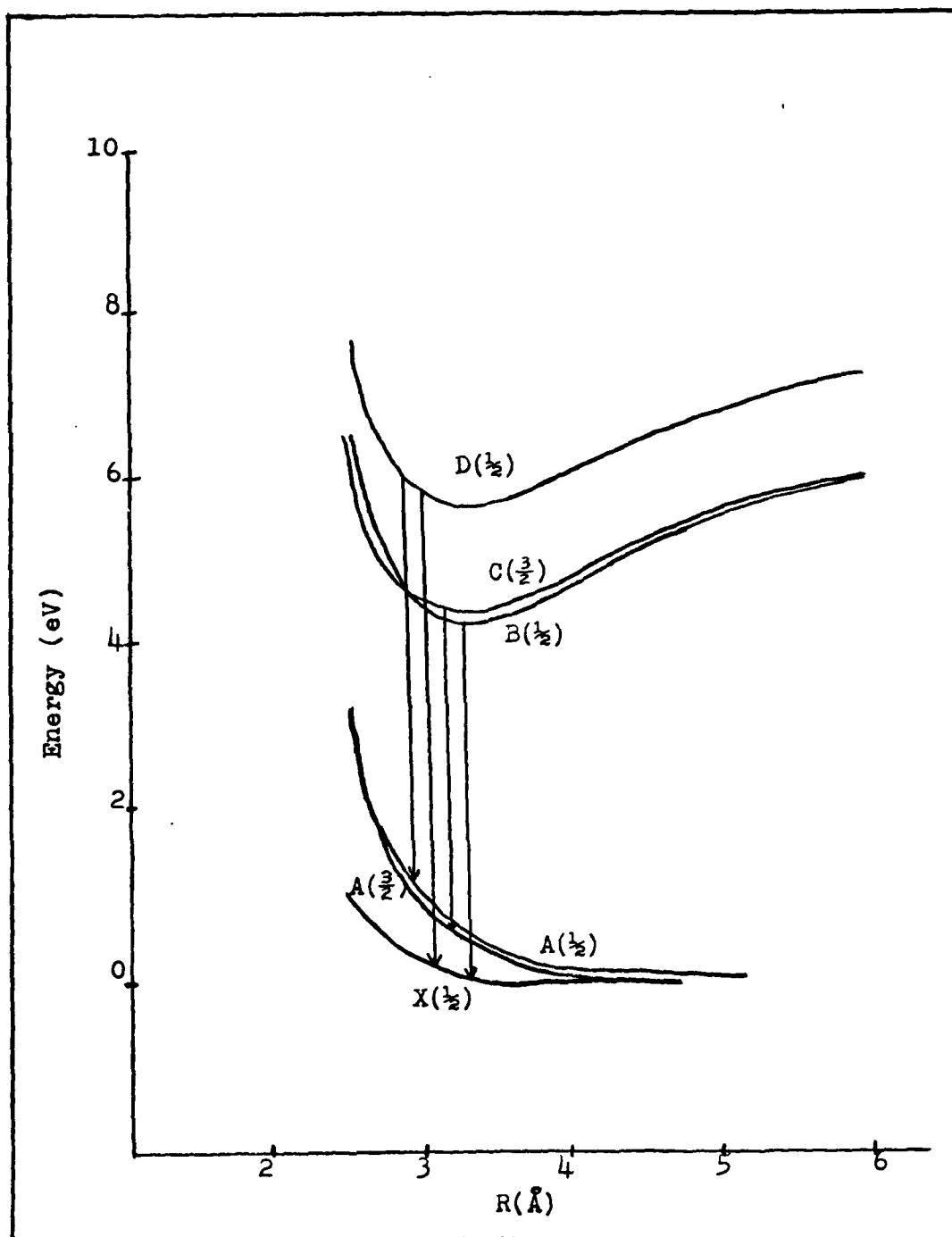


Fig 6. XeCl Potential Energy Curves and Allowed Transitions.

(Ref 10)

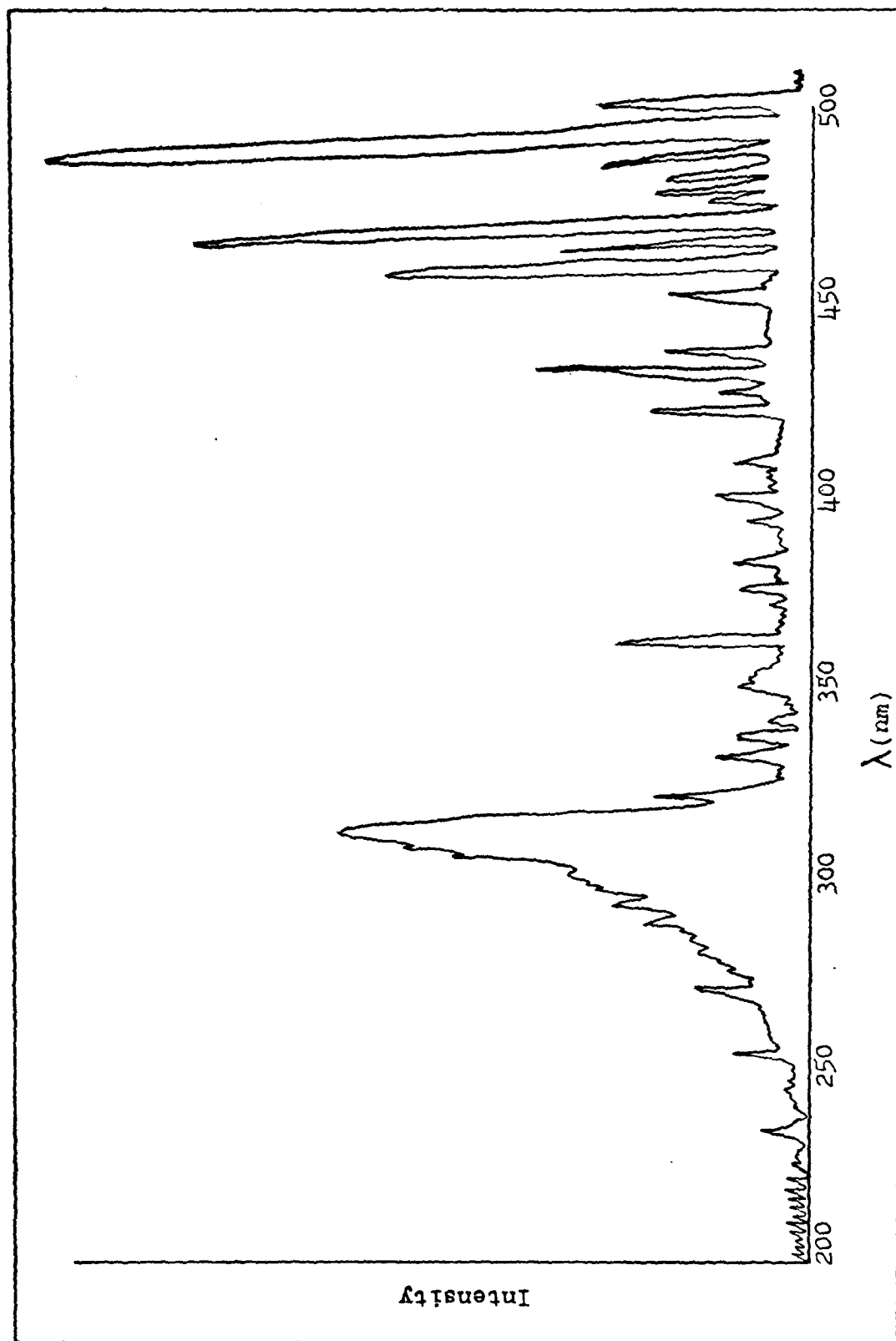


Fig 7. XeCl* Emission Spectra from a Hollow Cathode Discharge
of a Ne/Xe/HCl Gas Mix. (Ref 7)

$2\pi - 2\pi$ transitions, resulting from transitions to the repulsive A electronic state, are very weak (Refs 16 and 17). The D state, which mixes with the B state at close internuclear distances, can radiate to the X state (Ref 17). The $(D, \frac{1}{2} \rightarrow X, \frac{1}{2})$ transition occurs at 235.8 nm. The higher intensity spectral lines at wavelengths greater than 460 nm are due to atomic Xe transitions (Ref 18). Located at 450 nm are transitions due to Xe_2Cl^* (Ref 19).

As the pressure is increased, the short and long wavelength regions shift toward the main peak which becomes located at 308 nm, the main lasing transition for XeCl^* . The $(B, \frac{1}{2} \rightarrow X, \frac{1}{2})$ emission becomes more intense with increasing pressure because molecules in the $(C, \frac{3}{2})$ state are collisionally transferred to the $B, \frac{1}{2}$ state (Ref 14). The lasing radiative lifetime of the $(B, \frac{1}{2} \rightarrow X, \frac{1}{2})$ transition of XeCl^* has been measured to have a value of 16 nanoseconds (Ref 20). The XeCl^* spontaneous and laser emission spectrum are presented in Fig 8 for comparison (Ref 21).

Rare-gas halide laser mixtures consist of a dominant, lighter rare-gas used as the buffer gas in the discharge. A smaller amount of heavier rare-gas as compared to the buffer gas and a halogen donor species are used to form the lasing molecule. In the experiment, Ne was used as the buffer gas with HCl used as the halogen donor for Xe. The reaction kinetics involved in the plasma of a XeCl laser are not completely understood. Many chemical paths are possible for producing the XeCl^* lasing molecule, but which path is dominant under different current and pressure conditions of the plasma is still under investigation. The lack of understanding about the power degradation of the

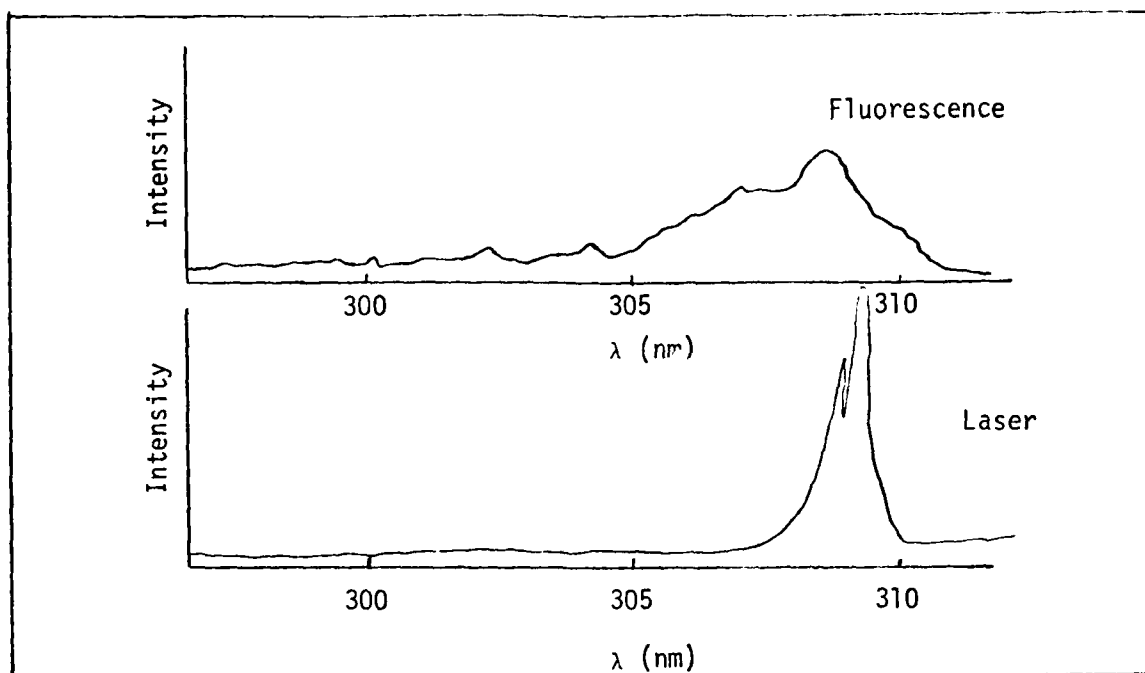


Fig 8. XeCl* Fluorescence and Laser Spectra
Under E-beam Excitation (Ref 21)

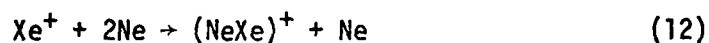
XeCl laser demonstrates the need to understand the quenching kinetics of XeCl* in the plasma. Reactions involved with determining the concentration of Cl₂ are important to unravel, due to the ability of Cl₂ to absorb the 308 nm lasing wavelength.

The discussion of the reaction kinetics begins with a presentation of the kinetics involved with forming excited rare-gas species, followed by a presentation of the reactions of these species with the halogen to form XeCl*. The quenching of XeCl* and XeCl is discussed along with a presentation of the photoabsorption processes involved in the discharge. The reaction thought to be most affected by the addition of H₂ is also presented.

The discussion of the excitation of the rare-gas species starts with the relevant electron impact excitation processes. The electrons undergo inelastic and ionization collisions with the lighter rare-gas of Ne, forming Ne^* and Ne^+ . To a much lesser extent, due to Xe being a minority species, the Xe suffers these collisions forming Xe^* and Xe^+ . These excited and ionized species can rapidly dimerize through the following reactions:



At low mol fractions of Xe, the Xe^+ and Xe^* can dimerize by two-step processes involving three body collisions with the light rare-gas buffer, such as:



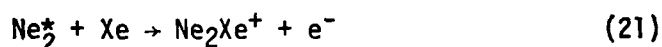
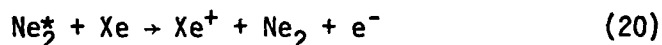
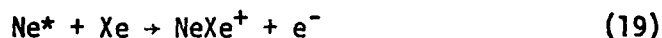
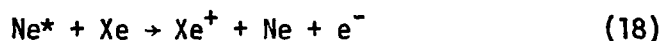
and



These three body processes are much faster than Eqs (10) and (11). The dimer ions can collide with electrons in dissociative recombination reactions of the type (Ref 22):



Interaction between the various xenon and neon species involves either energy or charge transfer between them. The energy transfer reactions are discussed first. If the Ne^* and Ne_2^* states are energetic enough, Penning or associative ionization of Xe may occur (Eqs (18) - (21):



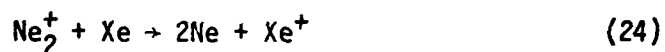
The first metastable state of Ne_2^* has sufficient energy to ionize Xe. Generally, Eqs (18) - (21) are gas kinetic ($\sim 10^{-10} \text{ cm}^3 \text{ s}^{-1}$), occurring at every collision if there is sufficient energy between the Ne^* and Ne_2^* with the Xe. If the Ne^* and Ne_2^* do not have enough excitation energy to produce associative or Penning ionization, these excited species may transfer their energy to the Xe by reactions of the type:



Reactions of the type like Eq (22) are generally slow unless there is a close resonance between the initial and final states of Ne^* and Xe. The rate of energy transfer between rare-gas atoms depends sensitively on the closeness of the resonance (Ref 23). A close resonance between initial and final states is not needed for reactions like Eq (23), so

these reactions are generally rapid ($\sim 10^{-10} \text{ cm}^3 \text{ s}^{-1}$) (Ref 24). The reason for reactions like Eq (23) occurring without the need for a close resonance of states involved in the energy transfer is that any excess energy can be carried away in the dissociation of the molecular species.

The HCD was never operated at pressures greater than 6 Torr. As a good approximation, due to the low operating pressures, the temperature of the gas species can be considered to be the same as the cathode wall temperature, which was near room temperature. Therefore, asymmetric charge transfer between ions can be ignored because this transfer process is generally slow at thermal energies. Charge transfer reactions from dimer ions to rare-gas atoms and molecules such as:



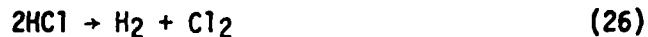
are generally fast.

The addition of the halogen bearing donor, HCl, to the mix allows the formation of the XeCl^* excimer. The halogen donor and the halogen itself undergo some reactions that will be discussed before the presentation of XeCl^* formation reactions. The HCl concentration in the discharge will eventually reach an equilibrium value. Naturally, the formation reaction of XeCl^* using the HCl is important in determining this equilibrium value, but the HCl can also undergo a dissociative attachment reaction like:



The H and Cl^- products of Eq (25) will eventually undergo reactions in the discharge to produce H_2 and Cl_2 respectively, giving an overall

reaction of the dissociation of HCl:



Cl_2 and Cl formed in the discharge may undergo exothermic dissociative attachment reactions like:



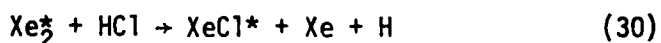
Reactions like Eq (27) are usually very rapid, with rate coefficients as great as $10^{-7} \text{ cm}^3 \text{ s}^{-1}$ at room temperature. The rate decreases somewhat at higher electron temperatures (Refs 25 and 26). A lower rate for a reaction of the type like Eq (27) would be expected in the hollow cathode due to the greater fraction of high energy electrons found in a hollow cathode as compared to a positive column discharge. There is little data available for halogens of interest in rare-gas monohalide lasers, but evidence seems to indicate that fluorine (F_2) has an exothermic dissociative attachment reaction rate coefficient on the order of $0.5\text{--}1.0 \times 10^{-9} \text{ cm}^3 \text{ s}^{-1}$ at an electron temperature of a few eV (Refs 27 and 28). A rate constant for Eq (28) at low pressures could not be found, but at total gas mix pressures of atmospheres, atomic fluorine (F) has a dissociative attachment rate constant estimated to be $1.0 \times 10^{-12} \text{ cm}^3 \text{ s}^{-1}$ (Ref 29). Cl probably has a comparable rate constant at high pressures.

The HCl and other halogen species can react with the excited and ionized rare-gas species to form rare-gas halide excimers. Through similar types of reactions to be presented for XeCl^* formation, the

various excited and ionized species of neon can react with the halogen or halogen donor to form NeCl^* and Ne_2Cl^* . The formation of XeCl^* due to the Xe^* produced by Eqs (17), (22), and (23) reacting directly with the HCl , is through the reaction:



This reaction was previously thought to be the dominant channel of formation for the upper laser level for discharges using HCl as the halogen donor, but recent results contradict this belief (Refs 11 and 14). The quenching rates and branching ratios for xenon metastable atoms $\text{Xe}(^3\text{P}_2)$ and $\text{Xe}(^3\text{P}_1)$ (the excited xenon states involved in formation of XeCl^*), with HCl as a halogen donor at low pressure were measured and branching ratios of .02 and .01 were found for $\text{Xe}(^3\text{P}_2)$ and $\text{Xe}(^3\text{P}_1)$ respectively (Refs 11 and 14). The low branching ratios for HCl as the quencher for xenon metastables at low pressure suggests that there is another more dominant reaction path leading to XeCl^* formation. Equation (29) has a rate constant of $5.6 \times 10^{-10} \text{ cm}^3 - \text{s}^{-1}$ for the $\text{Xe}(^3\text{P}_2)$ (Ref 14), but the rate constant for the $\text{Xe}(^3\text{P}_1)$ was not measured (Ref 11). The Xe_2^* product of Eqs (8), (10), and (15) may have reactions with the HCl of the type:



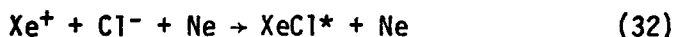
Xe_2Cl^* may also be formed through Eq (30) but since this molecule is not an important contributor to the lasing wavelength, it will not be discussed further.

The Xe* may also directly react with Cl₂ through the reaction:

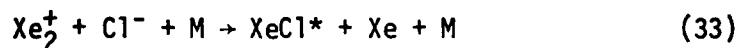


This reaction has a large cross section and near unit efficiency for producing excited products (Ref 30). Equation (31) has a rate constant of $7.2 \times 10^{-10} \text{ cm}^3 - \text{s}^{-1}$ for the Xe(³P₂) metastable (Ref 14), but the rate constant for the Xe(³P₁) could not be found. The reader may ask why is Cl₂ still a problem if it reacts so fast with Xe* to form XeCl*? Equation (31) cannot produce XeCl* any faster than Xe* is produced. The production of Xe* does not occur with the same large cross sections and efficiencies as Eq (31), so Eq (31) is limited by the Xe* production rate, allowing quantities of Cl₂ to remain in the discharge. The Cl product of Eq (31) can recombine with another Cl and form Cl₂ also.

The rare-gas positive ions can react with the Cl⁻ ions to form XeCl*. The Xe⁺ of Eqs (18) and (24) may react with Cl⁻ to form XeCl* via the reaction:

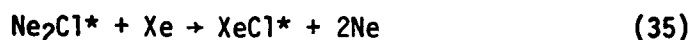


The Xe₂⁺ of Eqs (9), (11), and (13) form XeCl* through the reaction:



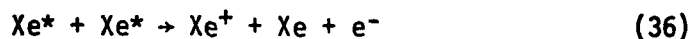
where M is some third body. Three-body recombination reactions of ions are extremely rapid. At low pressures ($\leq 1 \text{ atm}$), reactions like Eq (33) have rate coefficients on the order of $10^{-25} \text{ cm}^6 \text{ s}^{-1}$. The large rate coefficient is due to the long range Coulomb interactions of the ions (Ref 31). At pressures $\geq 1 \text{ atm}$, the rate coefficient

begins to decrease due to the larger number of particles in a volume that the ions must migrate through to get to one another (Ref 32). The rate coefficient for Eq (33) has never been measured. Finally, XeCl^* may also be formed from reactions with NeCl^* and Ne_2Cl^* via reactions of the type:



Reactions like Eq (34) are extremely fast, on the order of gas kinetic (Refs 33 and 34).

Just as the XeCl^* is formed by very rapid reactions, it is also quenched by rapid reactions. The Xe^* needed for the formation of XeCl^* can be quenched by electron impact (Refs 35 and 36). It can also be quenched by collisions with other Xe^* atoms through the reaction:



Quenching of XeCl^* can be possible by nearly all the species in the laser plasma, excluding maybe the heavy ions due to their low concentration. The dominant quenching process of rare-gas monohalide excimers in a low pressure discharge is direct quenching by the halogen bearing molecules, HCl and Cl_2 , via reactions of the type:

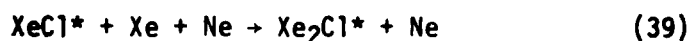


Equation (37) has a rate constant of $8 \times 10^{-10} \text{ cm}^3 \text{ s}^{-1}$ (Ref 20).

Equation (38) has a rate constant probably on the order of $10^{-9} \text{ cm}^3 \text{ s}^{-1}$.

Quenching of XeCl^* by the rare-gas atoms Xe and Ne is much slower than

quenching Eqs (37) and (38). At high pressures, the rare-gas atoms can quench the XeCl^* through three body reactions, such as (Refs 33 and 37):



Triatomic species as in Eq (40) have not yet been observed directly. Since the experiments were operated at low pressures (6 Torr or less) these reactions, Eqs (39) and 40), can be ignored (Ref 38). The electrons can quench XeCl^* through inelastic collisions. The electron quenching of XeCl^* is probably comparable to that of XeF^* (Ref 39).

The collisional dissociation of XeCl (X ground state) by Xe and HCl has been measured by Waynant and Eden (Ref 40). They measured rate constants of $(2.2 \pm 0.5) \times 10^{-11} \text{ cm}^3 \text{ s}^{-1}$ for HCl and $(5.6 \pm 0.8) \times 10^{-12} \text{ cm}^3 \text{ s}^{-1}$ for Xe for the dissociation of the XeCl ground state and found these rates to be independent of vibrational level. These small rate constants are contradictory to the efficiencies demonstrated by the XeCl^* laser. The lower laser level should depopulate very rapidly, contrary to the rate constants measured, due to the weak binding energy (255 cm^{-1}) of XeCl . These statements bear out the fact that rare-gas halide laser kinetics are not very well understood.

Several photoabsorption processes at the XeCl^* laser wavelength ($\lambda = 308 \text{ nm}$) can occur within the discharge, thus lowering the laser output power. The most dominant absorber in the XeCl^* laser system is the chlorine, due to the photodissociation reaction:



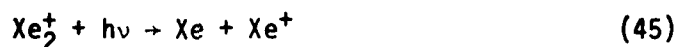
Other absorption processes include the photodetachment of negative ions like:



or the photoionization of excited rare-gas atoms and molecules through processes like:



or the photodissociation of the dimer ions of the rare-gas in processes like:



and XeCl can absorb the laser radiation. The available cross sections of some of the photoabsorption processes at 308 nm radiation are (Refs 41, 42, 43, 44, and 45):

$$\text{Cl}_2 \text{ --- } 1.7 \times 10^{-19} \text{ cm}^2$$

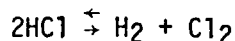
$$\text{Cl}^- \text{ --- } 2.2 \times 10^{-17} \text{ cm}^2$$

$$\text{Xe}_2^* \text{ --- } 1.4 \times 10^{-17} \text{ cm}^2$$

$$\text{Xe}_2^+ \text{ --- } 1.6 \times 10^{-17} \text{ cm}^2$$

Note that Cl₂ has the smallest cross section listed. Cl₂ is still considered to be the dominant absorber in typical rare-gas monohalide lasers due to the typically low species concentrations of Cl⁻, Xe^{*}, and Xe₂⁺. Therefore, it is advantageous to keep the Cl₂ concentrations as low as possible. It is not wise to lower the Xe^{*}, Xe₂^{*}, and Xe₂⁺ concentrations for they are critical in the formation of XeCl^{*}.

The addition of small amounts of H₂ to high pressure XeCl laser discharges has shown to have beneficial effects on the laser's performance, by maintaining the laser's high output power and lifetime. The basis of adding H₂ to the mixture revolves around the reaction of Eq (26) reproduced below:



It was hoped that through the addition of H₂, the reaction would be driven to the left, forming more HCl and depleting the Cl₂ concentration.

Table II lists some of the reactions mentioned in this section with their rate coefficients. If the rate for a XeCl* laser reaction was not known or available, a comparable reaction was listed along with the XeCl* laser reaction it represented. This was done to give the reader a knowledge of the magnitudes of the different types of reactions.

Hollow Cathode Discharge

The first rare-gas monohalide lasers used an electron beam to pump the media (Ref 21). Electron beams can supply the large number of high energy electrons needed to excite the rare-gas ions and metastables at a sufficient rate (the ionization potential and energy of the first metastable for Xe for example, are 12.1 and 8.4eV respectively (Ref 57:73)) for lasering to occur (Ref 58:1). Electron beams were also used for the reason that normal glow discharges could not be used at the high operating pressures of the rare-gas monohalide lasers, because the discharge would degrade into an arc. Electron beams are rather complex and expensive devices. Any other discharge system used

Table II
Some Reactions and Rate Constants for XeCl Discharges

Reaction	Rate	Ref No.
$\text{He}^* + 2\text{He} \rightarrow \text{He}_2^* + \text{He} \quad (\text{Ne}^* + 2\text{Ne} \rightarrow \text{Ne}_2^* + \text{Ne})$	2×10^{-34}	46
$\text{Ne}^+ + 2\text{Ne} \rightarrow \text{Ne}_2^+ + \text{Ne}$	$5.7 - 8.9 \times 10^{-32}$	47
$\text{Ne}_2^+ + e^- \rightarrow \text{Ne}^* + \text{Ne}$	$1.8 \times 10^{-7} \left(\frac{T_e}{300\text{K}}\right)^{-0.43}$	48
$\text{Xe}^* + 2\text{Xe} \rightarrow \text{Xe}_2^* + \text{Xe}$	4.0×10^{-32}	49
$\text{Xe}^+ + 2\text{Xe} \rightarrow \text{Xe}_2^+ + \text{Xe}$	2.0×10^{-31}	50
$\text{Xe}_2^+ + e^- \rightarrow \text{Xe}^* + \text{Xe}$	$1.4 \times 10^{-6} \left(\frac{T_e}{300\text{K}}\right)^{-0.5}$	51
$\text{Ar}^* + \text{Xe} \rightarrow \text{Xe}^* + \text{Ar} \quad (\text{Ne}^* + \text{Xe} \rightarrow \text{Ne} + \text{Xe}^*)$	2.1×10^{-10}	52
$\text{Ar}_2^* + \text{Xe} \rightarrow \text{Xe}^* + 2\text{Ar} \quad (\text{Ne}_2^* + \text{Xe} \rightarrow 2\text{Ne} + \text{Xe}^*)$	4.39×10^{-10}	53
$\text{Ne}_2^+ + \text{Kr} \rightarrow \text{Kr}^+ + 2\text{Ne} \quad (\text{Ne}_2^+ + \text{Xe} \rightarrow 2\text{Ne} + \text{Xe}^+)$	$\leq 5 \times 10^{-13} \quad (200\text{K})$	54
$\text{Xe}^+ + \text{Xe} + \text{He} \rightarrow \text{Xe}_2^+ + \text{He} \quad (\text{Xe}^+ + \text{Xe} + \text{Ne} \rightarrow \text{Xe}_2^+ + \text{Ne})$	1.1×10^{-31}	55
$\text{Xe}^* + \text{Xe} + \text{He} \rightarrow \text{Xe}_2^* + \text{He} \quad (\text{Xe}^* + \text{Xe} + \text{Ne} \rightarrow \text{Xe}_2^* + \text{Ne})$	1.4×10^{-32}	56
$\text{Xe}^* + \text{HCl} \rightarrow \text{XeCl}^* + \text{H}$	5.6×10^{-10}	14
$\text{Xe}^* + \text{Cl}_2 \rightarrow \text{XeCl}^* + \text{Cl}$	7.2×10^{-10}	14
$\text{XeCl}^* + \text{HCl} \rightarrow \text{products}$	8×10^{-10}	20

to pump rare-gas monohalide laser media would need to be able to supply enough high energy electrons to obtain ample excitation rates. The hollow cathode discharge (HCD) has a highly non-Maxwellian electron energy distribution (eed). This departure from a Maxwellian distribution results in an increase in the number of high energy electrons (Ref 59). Hollow cathode discharges have been used to pump a helium-fluorine laser (Ref 60) and rare-gas ion lasers (Refs 61, 62, 63, 64, 65, and 66).

The unique geometry of the HCD, as shown in Fig 9, gives rise to the non-Maxwellian eed. The gas to be excited is surrounded by the cathode fall of the discharge, allowing many high energy electrons to accelerate through the cathode fall voltage attaining a beam-like character. This is in contrast to the positive column of a normal glow discharge that has a nearly isotropic velocity distribution and relatively low average electron energies, approximately 1-2eV (Ref 68). A distinct advantage of the HCD over a normal glow discharge, is the HCD's ability to maintain a stable discharge in a medium containing an electronegative gas (Ref 67). The effect of electronegative gases in discharges will be discussed later.

Gas discharges in which the ionization of the gas is maintained without external aid are called self-sustaining discharges (Ref 69). Discharges that require external aid to maintain the ionization of the gas are called non self-sustaining discharges. An example of a non self-sustaining discharge is the e-beam, which injects high energy electrons into the discharge medium. Self-sustaining discharges typically consist of two planar electrodes inside a discharge tube filled with a gas at low pressure. A high voltage is placed across

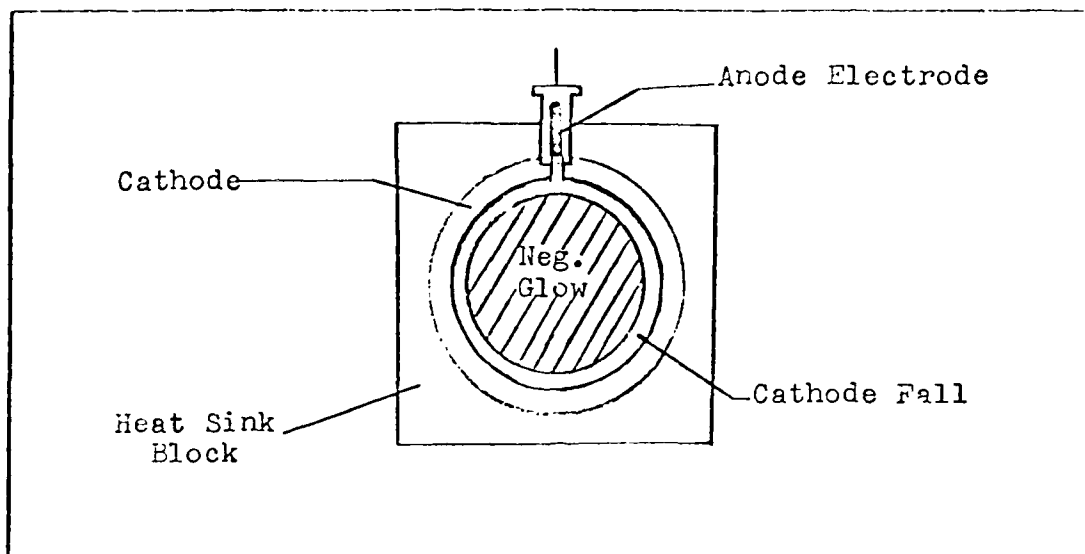


Fig 9. Characteristics of HCD used in Thesis Experiment (Ref 67)

the electrodes that accelerates a free electron to a high enough energy that the electron can ionize a gas molecule and cause an avalanche of electrons to the anode, making the gas conductive. There are three types of self-sustained discharges: the Townsend discharge, glow discharge, and the arc discharge. A voltage versus current representation of the characteristics of self-sustaining gas discharges is shown in Fig 10. The Townsend discharge does not have a large enough electron number density for efficient excitation rates of a laser medium and the arc discharge does not access enough of the laser medium. Therefore, laser discharges are operated under normal glow discharge conditions. As can be seen from Fig 10, the glow discharge operates at nearly a constant voltage over a wide range of currents (Ref 69). The current density in the cathode region of the discharge is maintained at a constant value because the discharge changes the active area of the cathode in response to any change in the total current (Ref 69).

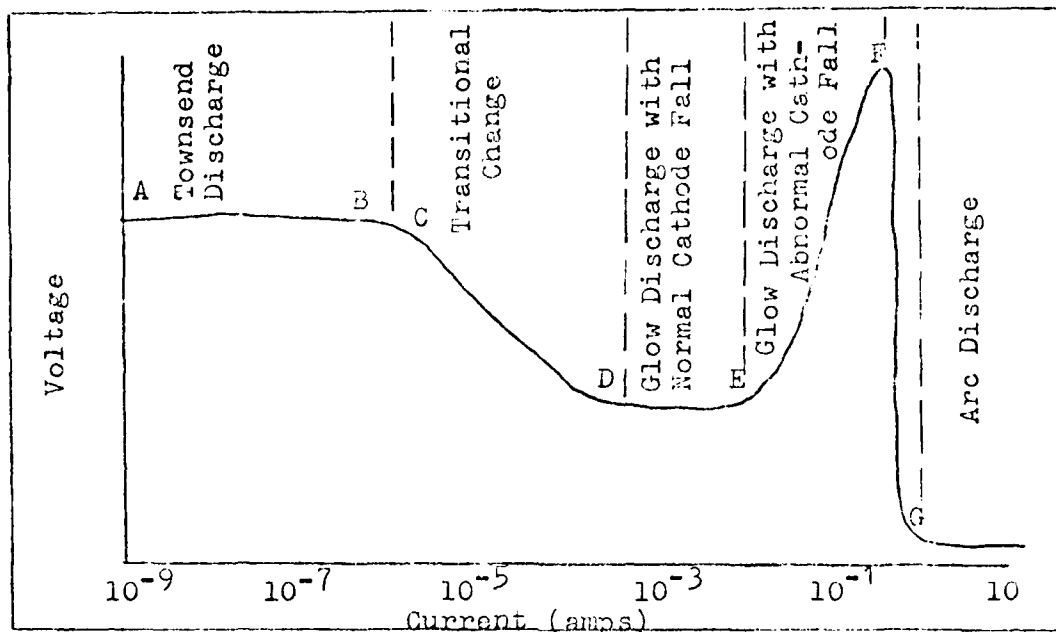


Fig 10. Characteristics of a Self-sustaining Gas Discharge (Ref 69)

The various fluorescent and dark areas seen in a discharge tube operating in the normal glow region, is shown in Fig 11. The various areas of the discharge will be discussed in succession, beginning at the cathode. Figure 11 also shows the variation of the electrical field, voltage, and also the electron and ion number densities through the length of the tube.

The Aston's dark space is due to secondary electrons ejected from the cathode by ion impact. These electrons are accelerated in the strong electric field present in the sheath (see Fig 11). The cathode glow identifies the region where the electrons are energetic enough to cause excitation of the gas molecules; the energy of the electrons in this region is the maximum of the excitation functions of the gas molecules. The electrons are further accelerated and in the cathode dark space cause ionization of the gas molecules. This lowers the

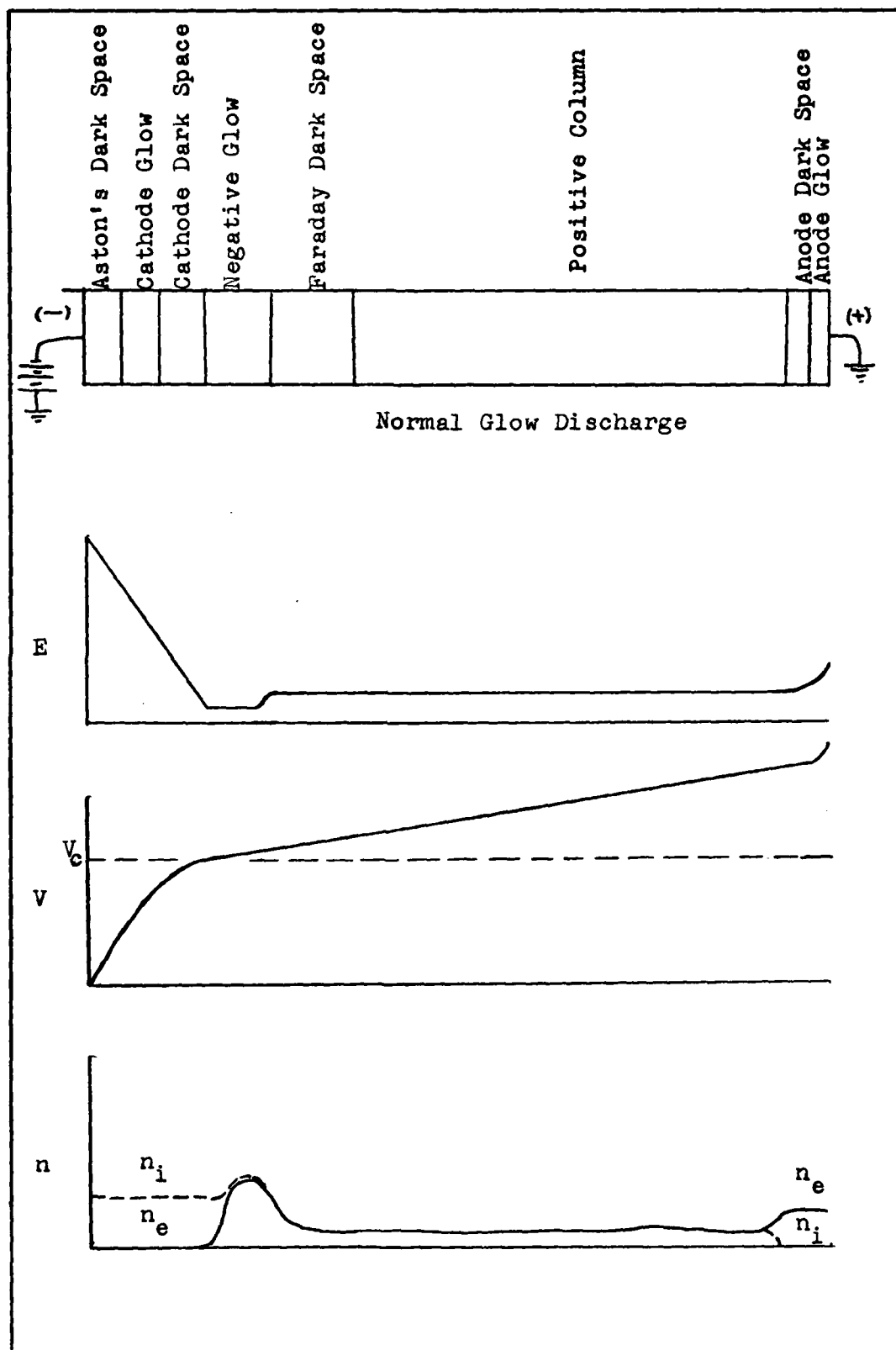


Fig 11. Luminous, Electrical, and Number Density Variations of a Normal Glow Discharge (Ref 57)

average electron energy. In the negative glow region there are frequent electron impact ionizations and excitations, dropping the average electron energy further. The Faraday dark space is due to the electrons not having enough energy to excite the atoms (Ref 69). Up through the Faraday dark space, the electrons have maintained a beam-like character. In the voltage plot of Fig 11, V_C is the cathode fall potential, which is the potential difference across the discharge from the cathode to the cathode dark space-negative glow boundary. The cathode fall has the largest potential gradient in the discharge. In Fig 10, from D to E, the voltage of the discharge is seen to be fairly constant. As stated before, as the current is increased in the normal glow region, the active area of the cathode grows keeping the voltage constant. This continues until the negative glow area is equal to the cathode area (Ref 69:45). Therefore, the normal glow region is also called the normal cathode fall region.

In the positive column, the electrons lose their beam-like character due to many elastic collisions. As can be seen in Fig 11, in this region there is nearly constant E , n_e , and n_i for the positive column region. The small voltage gradient of the positive column leads to an electron temperature of 1-2 eV and the heavy charged particles are maintained within a range of a few hundred degrees of room temperature (Ref 68). The glow is caused from random electron collisions with the gas molecules causing excitation of the gas. In this region, electrons carry most of the current due to their higher mobility and the magnitude of n_e is governed by the balance of electrons production and loss processes (Ref 68).

In the anode dark space, the electron velocity distribution assumes a beam-like character again due to their acceleration in the field of the anode. In the anode glow region, the electrons have gathered enough energy to excite and ionize the gas just before striking the anode. With this review of self-sustained discharges completed, a discussion of the hollow cathode discharge, which is also a self-sustained discharge, will be presented and contrasted with the positive column discharge.

There are several variations in design of HCD. For the experiment, a hollow metal cylinder was used as the cathode. The anode placement in this experiment is shown in Fig 9. In this cylindrical hollow cathode geometry, the negative glow is concentric with the cathode surface (Ref 67) and nearly fills the entire discharge cavity (Ref 60). Within this negative glow, the eed is highly non-Maxwellian, having a greater number of electrons of high energy than does a Maxwellian distribution. [As an example, Borodin and Kagan found a greater number of high energy electrons (>19.8 eV) in a hollow cathode discharge of He than in a similar positive column discharge (Ref 70)]. The reason for the larger number of high energy electrons in a hollow cathode is due to the negative glow's proximity to the cathode fall. Electrons ejected from the cathode are accelerated through the cathode fall and assume a beam-like character. The collisional excitation from this electron number density and energy distribution gives the intense light characteristics of the negative glow region. Electrons emitted from one side of the cylindrical cathode can penetrate the glow, enter the cathode, fall on the opposite side, and be repelled back into the

glow (Ref 59). Therefore, there is also increased ionization and excitation due to the oscillatory motion of the electrons within the tube.

An attempt to determine the actual electron distribution of a hollow cathode was made by P. Gill and C. E. Webb (Ref 59). They measured the electron energy distribution in the negative glow of a planar cathode abnormal glow discharge in He. The abnormal glow, while not an exact model of a hollow cathode discharge, still reveals the important features of both the hollow cathode and abnormal glow discharge. They used a differentially pumped retarding-field analyzer (Ref 59). Electrons from the negative glow would effuse through a sampling orifice in the anode into a low-pressure section that was continuously evacuated (Ref 59). For their experiment, the current, i , collected at any retarding potential V , is given by (Ref 71):

$$i = C n_e \int_V^{\infty} f(V) V^{1/2} dV \quad (46)$$

where

C = constant determined by the geometry of the orifice and screen, and the charge and mass of an electron.

n_e = the electron number density in the glow region sampled

$f(V)dV$ = normalized electron energy distribution giving the fraction of electrons with energies between eV and $e(V + dV)$.

If this expression is differentiated with respect to voltage, a quantity related to the eed can be found, i.e.

$$\left| \frac{di}{dV} \right| = C n_e f(V) V^{1/2} \quad (47)$$

The eed is usually expressed as $f(\epsilon)$, where ϵ is the energy of the electron in eV.

A v - i (retarding voltage versus collector current) plot from the Gill and Webb experiment is shown in Fig 12 for a pressure of 10 Torr, 3.5 mA discharge current, and an anode-cathode separation of 1.5 mm. Figure 13 shows the differentiated result. Note the presence of groups of high energy electrons. The plot shows three major components of the distribution:

1. At the full cathode fall energy of eV_C , there is an electron "Beam" component. The electrons in this component as a fraction of the total distribution were measured to be ~ 0.1 - 0.03 , at a pd value of ~ 1.57 Torr cm where p is the pressure of the discharge and d is the distance from the cathode.

2. There is a small peak in the distribution at eV_t after a small gap separating it from the "beam" component. This peak corresponds to electrons which have undergone one inelastic collision. The gap between eV_C and eV_t is approximately equal to the first excitation potential of the gas which is 20 eV for He. There is an appreciable tail of high energy electrons from eV_t down to low energies, ~ 26.4 eV. Graphical estimates yield values of 0.3 and 0.45 of the total number of electrons lie in this high energy tail. These values correspond to pd values of 1.5 Torr cm ($V_C = 190V$) and ~ 2.5 Torr cm ($V_C = 500V$) respectively.

3. The low energy component (< 50 eV) contains most of the electrons with most probable energies in the 5-10 eV range. Figure 14 shows the measurements of the low energy part of the electron energy distribution at different sampling distances from the cathode with the discharge operating at 10 Torr of He and 3.5 mA current. The maxima of the distributions are normalized to similar magnitudes.

The most probable energy of the distribution varies considerably with distance from the cathode. Figure 15 is a plot of the low-energy peak versus pd , for pressure in the range of 3-25 Torr with a discharge current of 3.5 mA. From Fig 15, it can be seen that within the negative glow (which for Gill and Webb was for $pd < 12$ Torr cm, the most probable energy starts ~ 1 eV near the Faraday dark space and rises to energies near 10 eV as the cathode dark space negative glow boundary

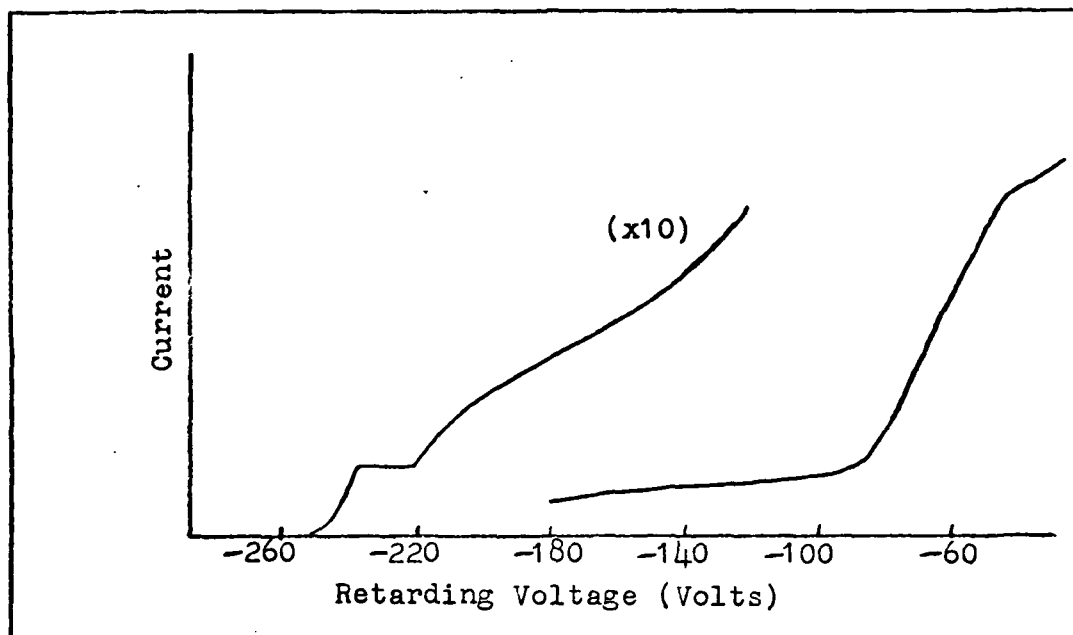


Fig 12. Retarding Voltage vs Collector Current (Ref 59)

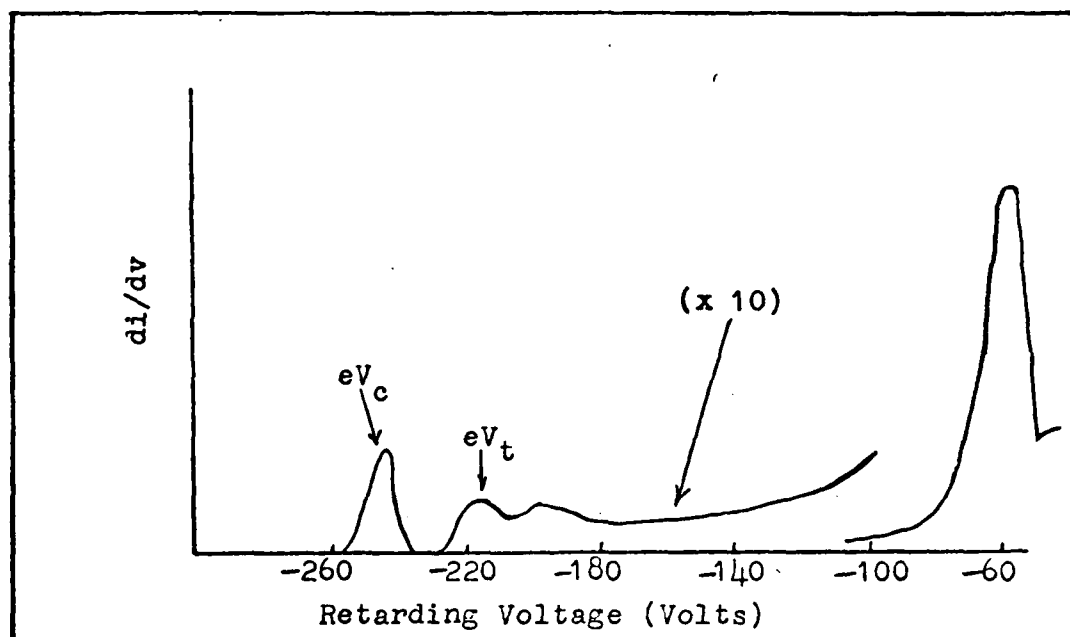


Fig 13. Differentiated Retarding Voltage vs Collector Current (Ref 59)

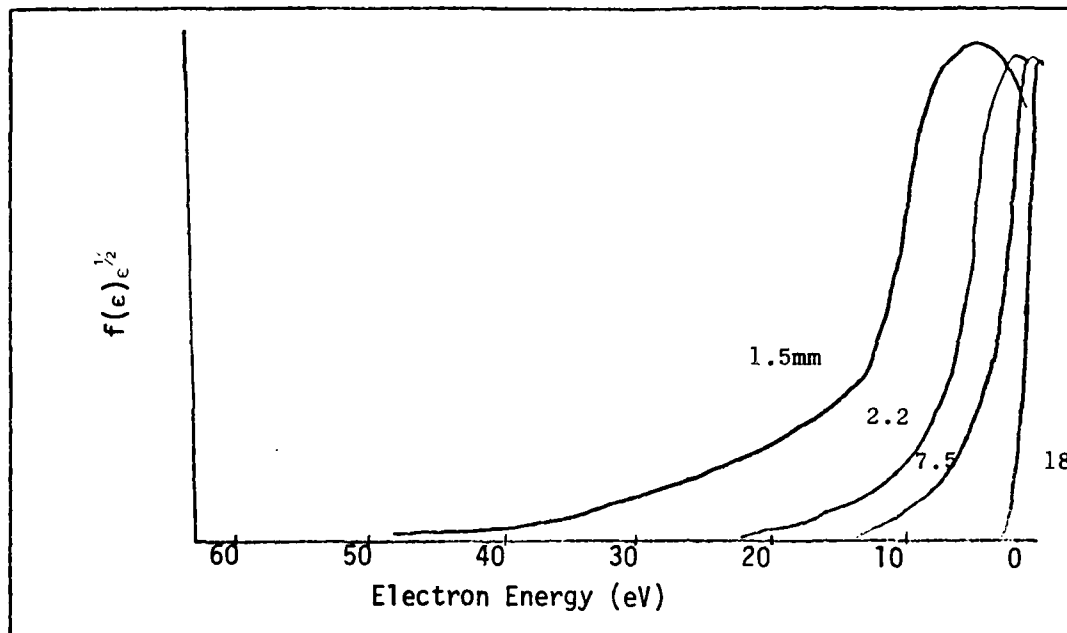


Fig 14. Low Energy Part of Electron Energy Distribution (Ref 59)

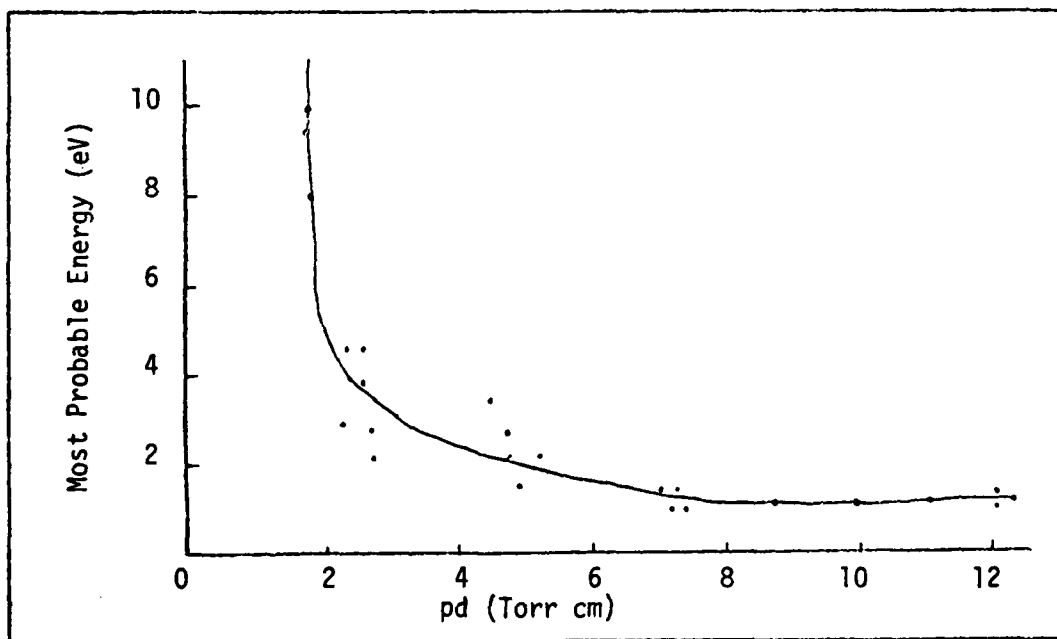


Fig 15. Low Energy Peak vs Pressure x Distance from Cathode (Pressure Ranges of 3-25 Torr and 3.5mA Discharge Current (Ref 59)

is approached. The cathode dark space negative glow boundary was further investigated by Gill and Webb.

The results of Gill and Webb show why the HCD is capable of providing the large number of high energy electrons needed for excitation of rare-gas monohalide laser media. A further advantage of the HCD is its ability to maintain a stable discharge in electronegative gases, such as Cl_2 and HCl (Ref 67). Positive column discharges in electronegative gases, in contrast, result in the occurrence of a wide variety of instabilities such as striations, streamers, and thermal arcing (Ref 67). In the negative glow region of a HCD, the ionization of neutrals is due to high energy electrons from the cathode fall. Also, there is weak electric field strengths in the negative glow (see Fig 11) and since ionization is by fast electrons, the stability of the discharge is not determined by the local field (Ref 67). Thus, electronegative gases can be used in large percentages in the hollow cathode discharge with the discharge remaining stable (Ref 67).

Photon Counting

A typical photon counting system is shown in Fig 16. The system consists of a photomultiplier tube, an amplifier, a discriminator, and a counter. The job of the photomultiplier is to convert the radiant energy into electrical energy and amplify it. The photomultiplier tube consists of two main sections, the photocathode and a series of dynodes (see Fig 17). Photons incident on the photocathode may cause the ejection of photoelectrons out of the photocathode and the electrons are accelerated by a potential difference through the dynode chain. The ratio of the number of photoelectrons emitted per incident photon

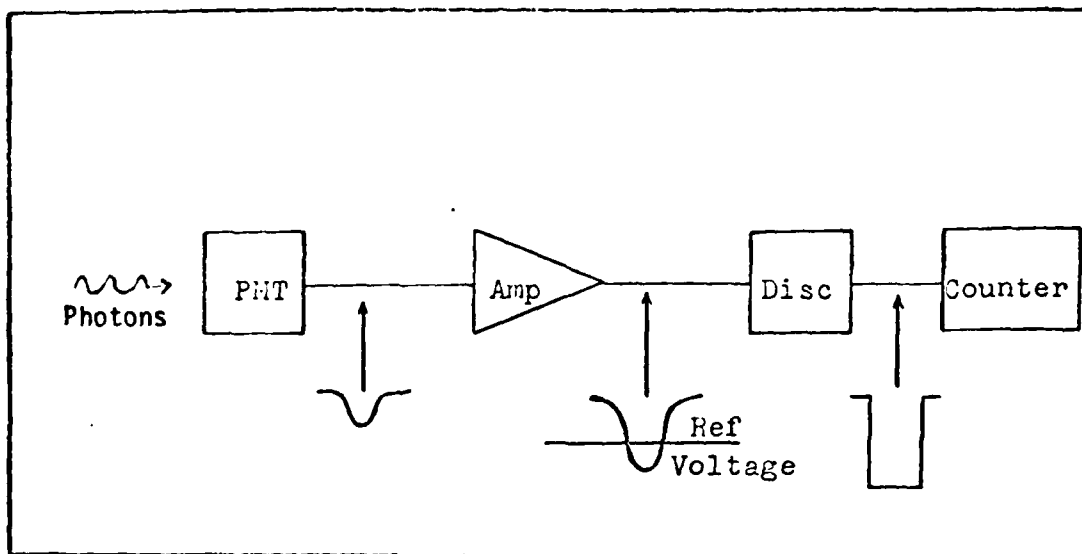


Fig 16. Photon Counting System (Ref 72)

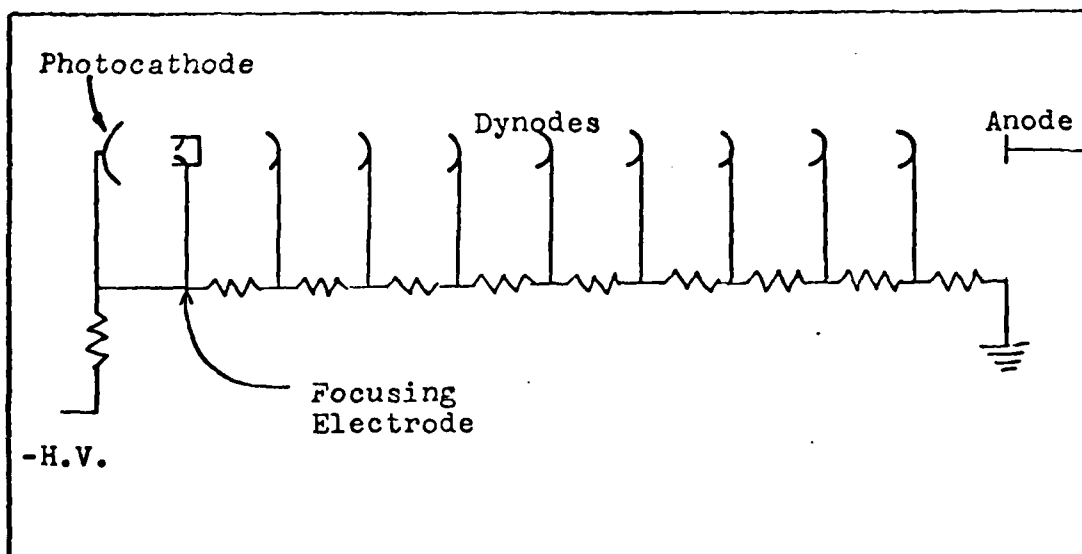


Fig 17. Structure of Photomultiplier Tubes (Ref 72)

is known as the quantum efficiency K . The material selected for use as the photocathode should have the highest quantum efficiency possible for the electromagnetic radiation being measured. Figure 18 gives the spectral response of several materials used as photocathodes. The plot is given as milliamps of output current per unit power of incident radiation on the photocathode as a function of wavelength, with the quantum efficiencies also given. Note the strong wavelength dependence. Table III lists some characteristics of some photocathodes. For the photons of the wavelength of interest to be counted, the photocathode with the highest spectral response for that wavelength should be chosen. Of the electrons leaving the photocathode, only some fraction X will strike the first dynode. If the number of photons per second striking the photocathode is given by n_p , then the number of electrical pulses at the photomultiplier output N_e , in time t , is given by (Ref 74):

$$N_e = n_p K X t \quad (48)$$

or

$$N_e = W(h\nu)^{-1} K X t \quad (49)$$

where

W = power of the incoming radiation

$h = 6.63 \times 10^{-34}$ Joules-sec, Planck's constant

ν = frequency of the incoming radiation

A problem encountered with all photomultiplier tubes is the dark current, which is present even when its PMT is operated in darkness. Dark current is extraneous pulses to go through the photomultiplier

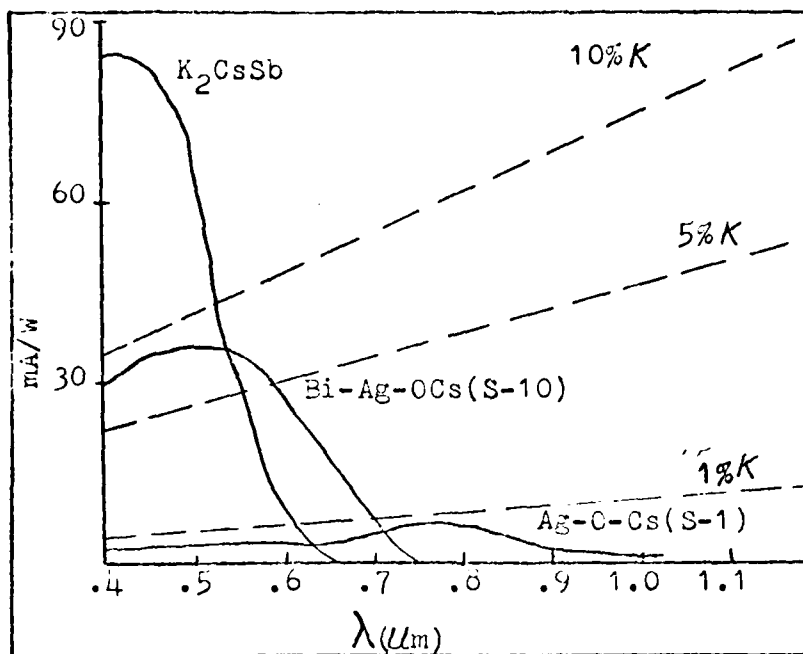


Fig 18. Spectral Response of Some Photocathodes (Ref 74)

tube, and if low light levels are being measured, can give erroneous results. The main source of dark current is from thermionic emission of electrons from the photocathode. Richardson's equation (Ref 75)

$$I_t = 1.20 \times 10^2 T^2 \exp((-1.16 \times 10^4)T^{-1}\theta_t) \text{ Amp cm}^{-2} \quad (50)$$

where

I_t = the thermal dark current

T = absolute temperature in $^{\circ}K$

θ_t = thermal work function

governs approximately the dark current. From Eq (50) it is obvious that the cooling of the photomultiplier will reduce the dark current. Residual dark current consists mostly of multiple electron pulses due mostly to photons produced in the photomultiplier window from the

Table III

Characteristics of Some Photocathodes (Ref 73)

Cathode Type	Composition	Peak λ	Typical K (λ peak)	Typical $\frac{mA}{W}$
S-20	$Na_2KSb-Cs$	3800	0.22	67.5
S-11	Cs_3Sb-O	3900	0.19	59.8
S-10	$BiAgOCs$	4200	0.068	23.0
Bialkali (ambient temp.)	K_2CsSb	3800	0.27	82.8

passage of relativistic particles from the disintegration of radioactive particles naturally occurring on the windows (Ref 73). Also, ions from absorbed gases on the tube and electrodes may generate pulses (Ref 74). The dark current puts a lower limit on the level of light which can be accurately measured by the photomultiplier.

The electrical pulse that reaches the first dynode is extremely weak and probably could never be measured directly. The purpose of the remaining dynodes is to amplify this signal. As the photoelectrons strike the first dynode, more electrons may be ejected out of the first dynode than struck it. The dynode is made of metals that enhance the secondary emission of electrons. These secondary electrons are accelerated to the second dynode due to the high negative biasing voltage applied to the photomultiplier (see Fig 17). This process continues with the pulse being amplified by each successive dynode. The negative voltage biasing allows better matching to an output coaxial cable and less electrical shock hazard. The dynode-resistor network provides the

correct accelerating potentials. The proper voltage should be chosen such as to maximize the pulse amplitude, but not to the point of increasing thermal heating, thereby creating more dark current. The electrons from thermal heating can cause erroneous counts and poor signal to noise ratios. Due to the slightly varying paths of the individual electrons through the dynode chain, they will have differing transit times. The varying transit times will cause the electrical pulse to have a finite width. For typical photomultipliers, the full width at half maximum (FWHM) of the pulse varies from 5-20 ns (Ref 72). The total gain G for the photomultiplier is given by (Ref 75)

$$G = X (g\delta)^n \quad (51)$$

where

X = fraction of photoelectrons emitted from photocathode that strike the first dynode

g = the transfer efficiency of electrons between dynodes

δ = average secondary emission coefficient of the dynodes

n = the number of dynodes

The pulse, after being amplified by the dynode chain, leaves the anode of the photomultiplier and goes to the amplifier (see Fig 16). The amplifier amplifies the signal a specific amount and sends it to the discriminator. The discriminator compares the peak value of the pulse to a reference voltage. If the pulse peak is greater than the reference voltage, the discriminator puts out a standard pulse to the counter to be counted. If the peak of the pulse from the photomultiplier is less than the reference voltage, the discriminator sends no pulse to the counter. The reference voltage is set so as to keep the dark current counts as low as possible.

If the intensity of the light source is increased, the average rate of emission of photons is also raised. Assuming that the light source emits photons according to a Poisson distribution, the probability that n photons will strike the photocathode in a time t is (Ref 72):

$$P(n,t) = \frac{(Rt)^n e^{-Rt}}{n!} \quad (52)$$

where

R = average photon emission rate

Likewise, the resulting number of photoelectrons given off by the photocathode is (Ref 72)

$$P(n,t) = \frac{(KRt)^n e^{-KRt}}{n!} \quad (53)$$

All detectors, such as the photomultiplier, have some resolving time t_r , due to their non-zero response times to signals. Typical PMTs have t_r 's of 10-40 nsec. If two photoelectrons are emitted from the photocathode at times less than t_r , one large and wider pulse will pass through the photomultiplier instead of two. This phenomenon called pulse pile-up occurs more and more as the photon rate is increased. The error due to pulse pile-up is computed as follows. Still assuming a Poisson distribution, the output pulse rate R_0 , with pulses from the detector being separated by a time t_r , is given by (Ref 72):

$$\begin{aligned} R_0 &= KR \cdot P(0,t_r) \\ &= KR \cdot e^{-KRt_r} \end{aligned} \quad (54)$$

This gives a pulse pile-up error E_{PMT} , of (letting $R_i = KR$) (Ref 72):

$$\begin{aligned} E_{PMT} &= \frac{R_i - R_o}{R_i} \\ &= \frac{R_i - R_i e^{-R_i t_r}}{R_i} \\ &= 1 - e^{-KR t_r} \end{aligned} \quad (55)$$

The discriminator can also cause errors due to pulse pile-up. There is a "dead time" t_d , of the discriminator where the discriminator will not accept any incoming pulses while it runs through the process of comparing the input signal with the reference voltage and generating a standard pulse. This dead time is essentially constant. The number of incoming pulses arriving at the discriminator in a time t is $R_i t$. The number of output pulses is $R_o t$. The total dead time of the discriminator is $R_o t t_d$. The output count will equal the input pulse rate times the time when the discriminator is counting pulses, or (Ref 72):

$$R_o t = R_i (t - R_o t t_d) \quad (56)$$

So that (Ref 72):

$$R_i = \frac{R_o}{1 - R_o t_d} \quad (57)$$

The error due to pulse pile-up from the discriminator is (Ref 72):

$$\begin{aligned} E_{DIS} &= \frac{R_i - R_o}{R_i} \\ &= R_o t_d \end{aligned} \quad (58)$$

Figure 19 shows the relationship between R_o and R_i , the output and input count rates respectively, for photomultipliers and discriminators.

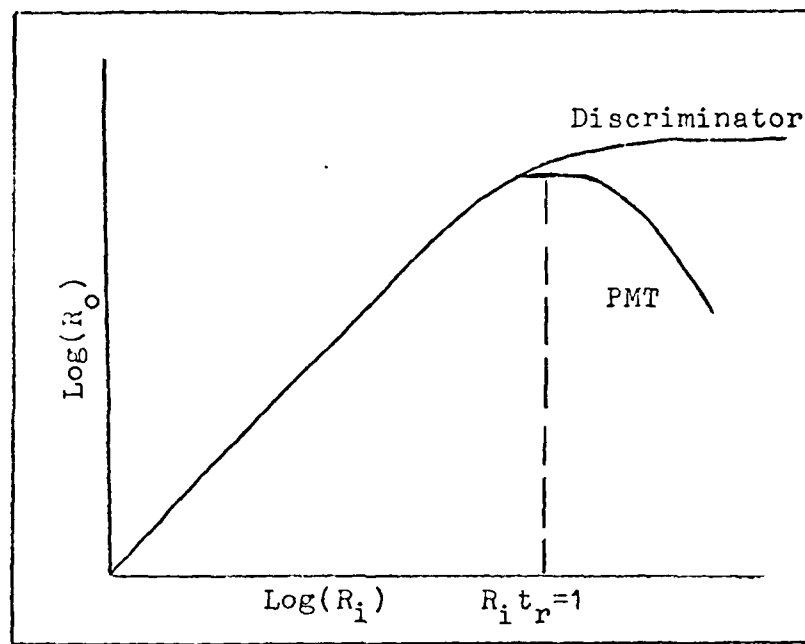


Fig 19. Input and Output Rates for Photomultipliers and Discriminators (Ref 72)

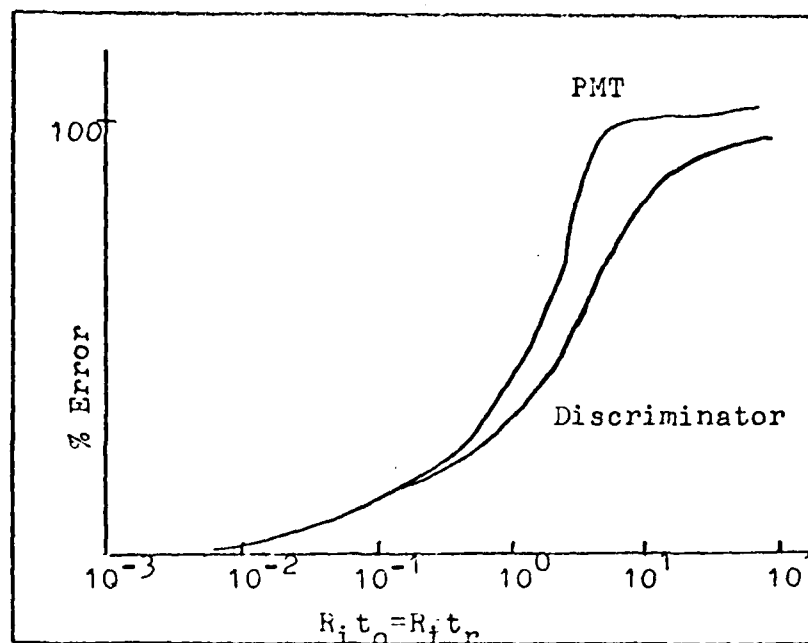


Fig 20. Error Due to Pulse Pile-up for Photomultipliers and Discriminators Ref 72)

Figure 20 shows the percentage of error due to pulse pile-up for photomultipliers and discriminators.

Even if conditions are such that the errors just discussed are small, a fundamental uncertainty exists in the counting of photons, due to the statistical and discrete nature of photons and electrons. Assuming the distribution of photoelectrons given by Eq (53), the average number of photoelectrons, N , emitted in a time t , is given by:

$$N = KRt \quad (59)$$

The noise or uncertainty in N is given by σ , the standard deviation of the distribution which is:

$$\begin{aligned} \sigma &= \sqrt{KRt} \\ &= \sqrt{N} \end{aligned} \quad (60)$$

Neglecting thermionic emission and pulse pile-up errors, the signal to noise ratio for a photomultiplier is:

$$\begin{aligned} \text{SNR} &= \frac{KRt}{\sqrt{KRt}} \\ &= \sqrt{N} \end{aligned} \quad (61)$$

III. Experimental Apparatus and Approach

The arrangement and electrical connections of the equipment used in this experiment are shown in Fig 21. A detailed drawing of the vacuum system and hollow cathode discharge tube is shown in Fig 22. The system was built to maintain high vacuum (base pressure of 10^{-6} Torr) conditions with all connections being made of stainless steel and copper gasket seals were used throughout the system. No O-rings were used. A Welch Scientific Model 1397 pump was used to rough out the system. To attain the high vacuum conditions, a Granville-Phillips Series 205 diffusion pump fitted with a liquid nitrogen cold trap was used.

All valves used on the experimental apparatus were of high vacuum quality so as to maintain the high vacuum integrity of the system. The butterfly valves used rubber gaskets to close off the gas flow inside the valve body, but had welded bellows seals to the outside air. These valves were only used when mixing a large amount of gas which was to be stored in a bottle for later use, and the valves were never used when running an experiment. The copper seal bellows valve mounted on the hollow cathode discharge tube was placed in the system to stop the diffusion of any HCl into the hollow cathode from the pumping station while an experiment was in progress. This type of valve was chosen primarily because it has the large throughput needed to pump down the HCD tube to the 10^{-5} Torr range between runs. The bellows valve on the other side of the hollow cathode from the copper seal bellows was used to open and close the hollow cathode to the roughing pump. The needle

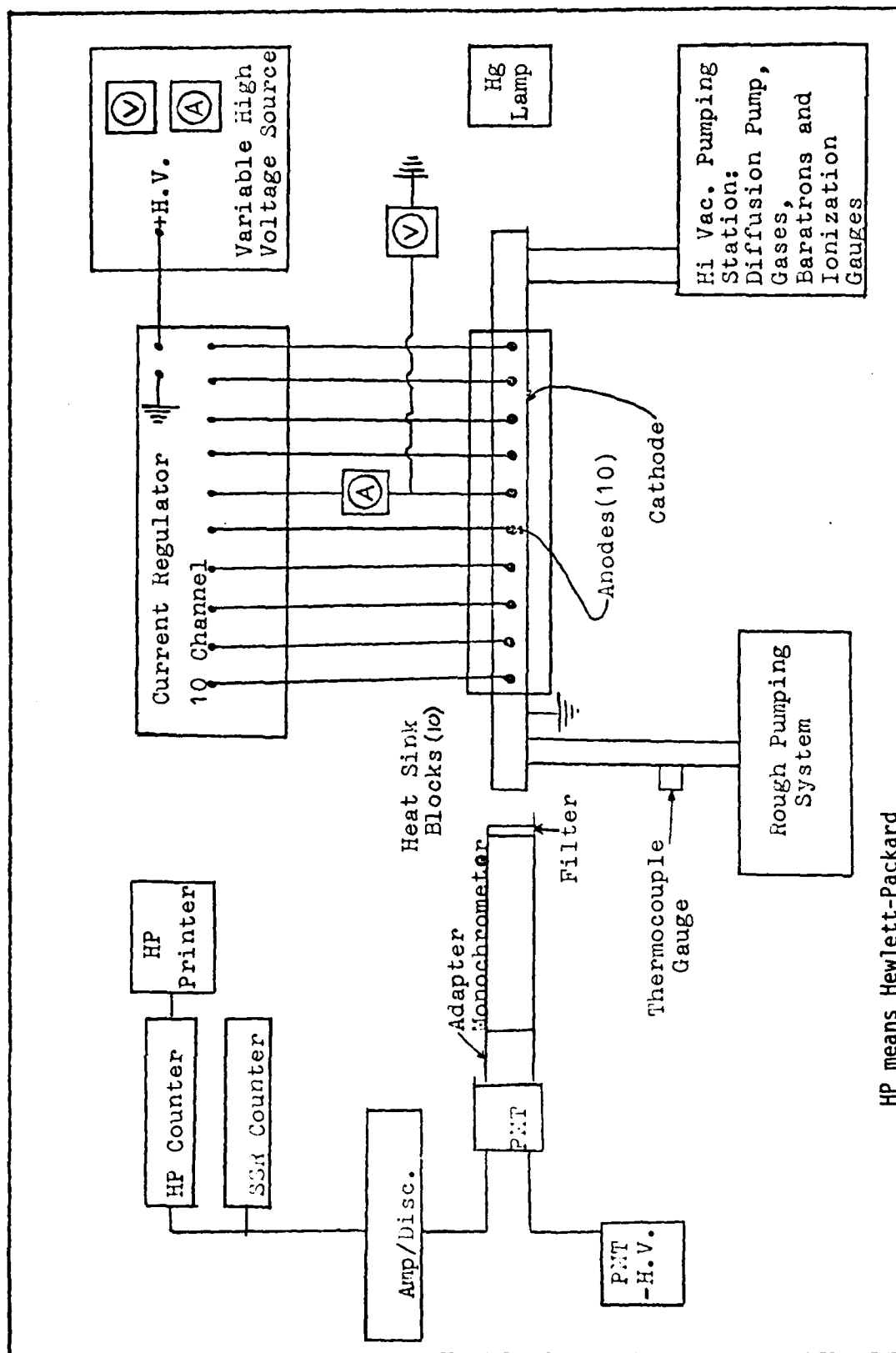


Fig 21. Equipment Arrangement of Thelst Experiment

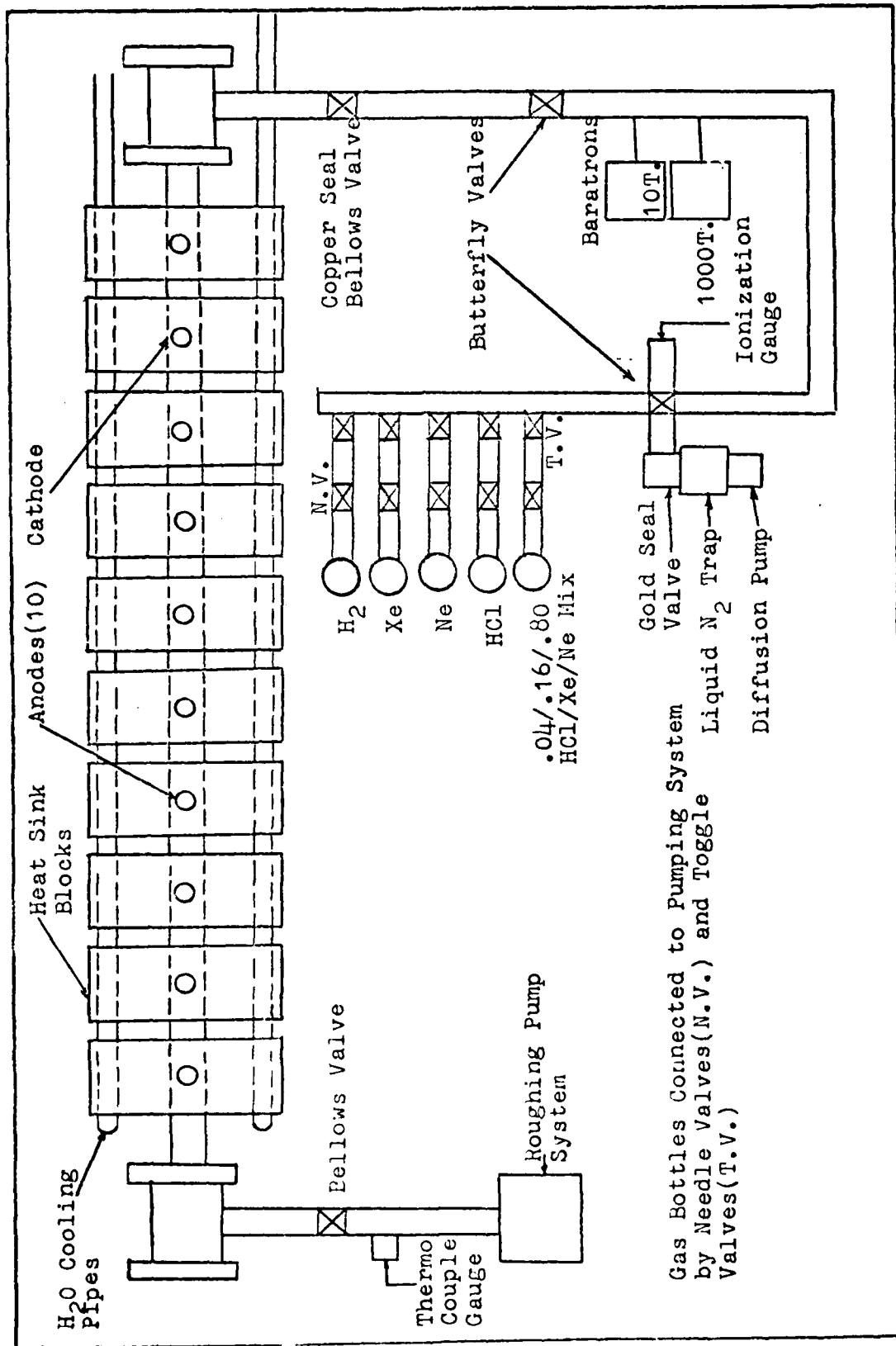


Fig 22. Vacuum System and Hollow Cathode Discharge Tube Used in Experiment

and toggle valves employed by the pumping station for filling into the system were also of high vacuum quality.

The placement of the various pressure gauges used for the experiments are shown in Fig 22. Two MKS Baratron gauges were used. These were 10 Torr head (145BHS-10) and a 1000 Torr head (315BHS-1000). The 10 Torr Baratron was used to measure the gas pressure in the HCD tube during the tube's static filling with the gas mixture. The 1000 Torr Baratron was used only when making large amounts of a pre-mixed gas. When pressures in the system went below 1×10^{-3} Torr during pumping with the diffusion pump, the pressure was measured with a Varian "nude" Baird-Alpert ionization gauge. The gauge was read out using a Perkin Elmer Digital Ionization gauge, Model 605-0000. The nude gauge was housed in a 1-1/2" inner diameter stainless steel nipple. The thermocouple gauge on the roughing line was a VEECO, Model D62-2T. This gauge was used to monitor the pressure inside the roughing line when the cathode was being roughed down.

A schematic of the hollow cathode discharge tube is shown in Figs 22 and 23. The hollow cathode itself is 61.595 cm in length, and is 78 cm long including the extensions for pumping connections. It has an inside diameter of 0.775 cm and is constructed of stainless steel. There are 10 stainless steel anodes attached to the cathode and insulated from it by alumina (see Fig 9). The anode ends 0.556 cm from the inside diameter of the cathode. The anodes are equally spaced from one another by 5.715 cm. Surrounding the cathode and the lower portion of each anode are 10 heat sink blocks made of aluminum. The two end blocks are 3.810 cm x 3.810 cm x 5.398 cm and the remaining blocks are

5.080 cm x 3.810 cm x 5.398 cm. The blocks are separated from each other by 0.635 cm. Running through the heat sink blocks are a pair of copper pipes on either side of the tube. These were for the flow and return of the water used for carrying away the heat the blocks absorbed from the discharge tube (see Figs 22 and 23).

The windows on either end of the cathode (see Fig 23) were made of sapphire. Sapphire windows were chosen because sapphire transmits U.V. radiation readily. To obtain an estimate of the temperature of the hollow cathode walls, a mercury thermometer was placed on top of a heat sink block.

Voltage was supplied to the hollow cathode by a variable voltage Gregory-King Electronics 3 kilowatt power supply. This unit has a built-in voltmeter and ammeter so that total voltage and current of the power supply could be monitored. The power supply was connected to a ten channel current regulator that was constructed at the Air Force Propulsion Laboratory. The current regulator maintained a constant current flowing through each anode. The current through one of the anodes was monitored by an ammeter connected in series with one of the electrodes. A voltmeter was connected between this same anode and ground. This was to measure the potential difference between the anode and cathode, the cathode being at ground potential.

The absorption of U.V. radiation by Cl_2 was in the experimental technique used to determine the Cl_2 concentrations. The U.V. radiation was supplied by a GEH100A4/T low pressure mercury lamp powered by a Gates Laboratory Arc 60 cycle A.C. power supply. To enhance the signal to noise ratio of the measurement, two things were done.

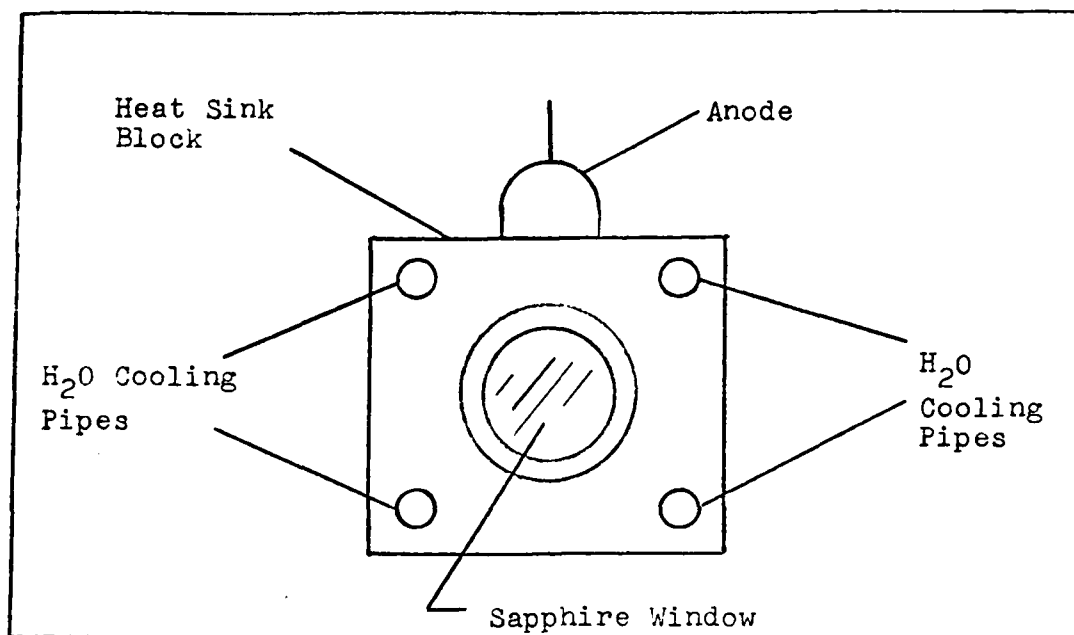


Fig 23. End View of Hollow Cathode Discharge Tube

First, black tape was wrapped around the end of the tube and the monochromator to give a light tight channel for the U.V. radiation from the discharge to pass through and also to cut out stray light from the room. Second, depending on what spectral line was being used from the mercury source for the absorption spectroscopy, either the 3131\AA or 3650\AA lines, the appropriate narrow band filter was used. The filters used were Oriel interference filters of the appropriate wavelengths. The first few experiments were run using the 3131\AA line, due to Cl_2 large cross section for absorption of this wavelength of radiation. Later, it was felt that some of the strong emission band centered near 308 nm of XeCl^* was being passed through the filter. It was then decided to use the 3650\AA line for the absorption spectroscopy and the appropriate filter. The monochromator used was an American Instruments SA, Model H-20 U.V. $1/4\text{-m}$ monochromator. The monochromator utilized a holographic grating. Various slit widths and heights were tried on

the monochromator to optimize the intensity of the signal entering the photomultiplier. It was found that no combination of slit widths and heights altered the intensity of the signal significantly. It was decided to use the 0.5mm width slits and the smallest height adjustment so as to enhance the resolution of the system.

The photomultiplier tube (PMT) used was an EMI 6256SA. It has 13 venetian blind dynodes made of CsSb. The tube is fitted with a spectroasil window and the overall spectral response is S-13. The base wiring of the photomultiplier tube had to be extensively modified (see Fig 24). One modification that had to be done was due to a bad Zener diode that caused large amounts of noise and washed out any signal. Two new Zeners were put in to replace the defective one. Two were used so as to handle the voltage of the PMT. There was still enough noise in the system to wash out the change in the photon count due to absorption by the Cl_2 . This was corrected by adding the several capacitors to the PMT with the values as shown in Fig 24.

The determination of the proper operating (bias) voltage of the photomultiplier was done in a two part experiment (Ref 76:2.5 - 2.9). This experiment started by having the photomultiplier blocked off from all light and voltages from 900 to 1600 volts in 50 volt increments were applied to the tube and the dark current counts were measured. Then, light giving counts approximately 100 times greater than the dark count was admitted into the photomultiplier and the biasing voltage was varied as before. The two resulting plots are shown in Fig 25. In determining the appropriate biasing voltage to use, the number of counts anticipated in the experiment has to be considered.

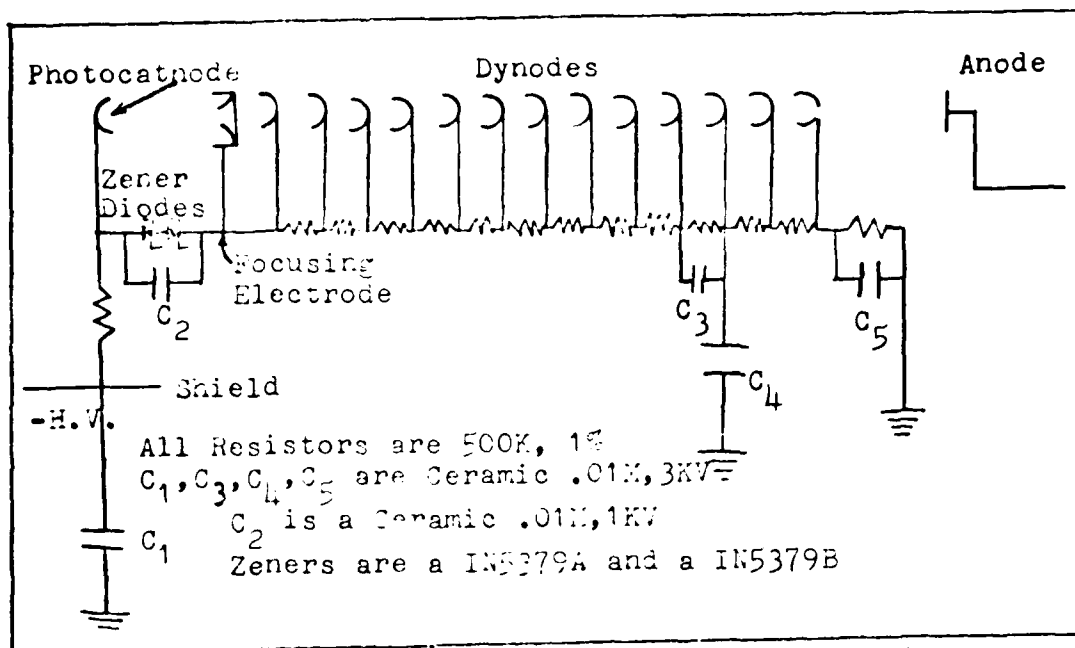


Fig 24. Wiring Diagram of PMT Used in Thesis Experiment

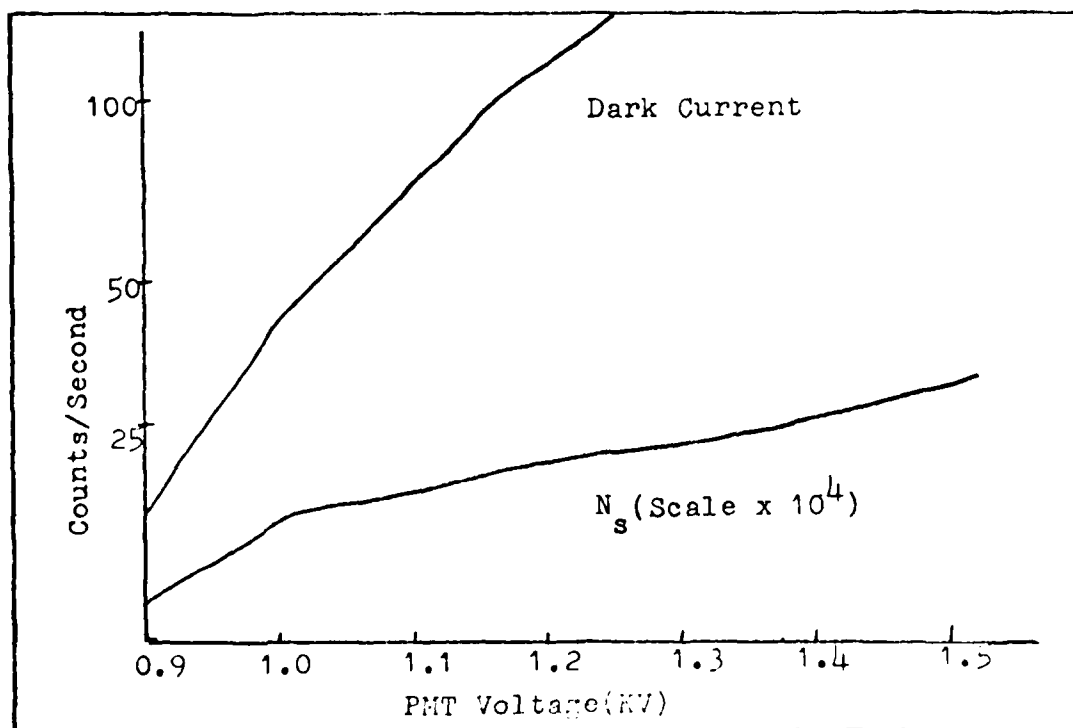


Fig 25. Dark and Light Source Counts Used in Determining PMT Biasing Voltage

It was desired to attain the greatest accuracy possible, requiring as many counts as possible from the source (assuming a Poisson distribution of photons from the source, the standard deviation of the measurement is the square root of the counts). Therefore, the counts from the source would be much greater than the dark counts. For this reason, the operating voltage is obtained from the flattest portion of the light source count curve, N_s . This criteria is desirable for two reasons (Ref 76:2.7):

1. It minimizes variations in effective calibrations with changes in multiplier gain; and
2. avoids counting spurious pulses and after-pulses which cause the rise in the N_s curve at high operating voltages.

From this experiment, the operating voltage was determined to be 1050V. If light levels comparable to the dark count were to be measured, the optimum operating voltage is found at the point where the slope of the logarithm of the dark count is twice the slope of the light source's count logarithm. This is the point where the signal to noise ratio is optimum (Ref 76:2.7).

The number of counts per second of U.V. radiation from the mercury lamp when the photomultiplier was biased with 1050V was on the order of 5.0×10^6 . An experiment was done to ensure that the photomultiplier was operating in a linear fashion, i.e., that the counts from a source A plus counts from a source B did in fact equal counts from A plus B (see Fig 19). With the monochromator set at 3131\AA , the mercury lamp source and another U.V. source were allowed to shine on the photomultiplier together and then separately. This was done several times with varying bias voltages. It was found that the counts had to

be no greater than 1.2×10^6 counts/sec. to still have the PMT operating in a linear fashion. To maintain this order of counts with the mercury source, a bias voltage of 885 volts was used. The source for this biasing voltage was a Hewlett-Packard Model 6110A D.C. power source.

The signal from the photomultiplier was sent into a SSR Instrument Model 1120 Amplifier-Discriminator which was connected to a SSR Instrument Model 1110 Digital Synchronous Computer counter. The SSR counter gave only a three digit display. Greater accuracy was needed, so an eight digit Hewlett-Packard Model 5248M counter was placed in parallel with the SSR counter. The SSR counter was still needed to drive the amplifier-discriminator. The Hewlett-Packard counter was connected to a Hewlett-Packard Model 5050B digital printer which has a six digit capacity. Since the counts/sec during an experiment was not going to exceed a value of 1.2×10^6 , the printer was capable of handling all measurements. The counter was operated throughout the thesis in the one second counting interval mode.

A standard mixture of gas was used throughout the experiments. Upon examination of spectra of XeCl^* in the hollow cathode taken by George Vogel, the most intense emission of XeCl^* was found to be from a mixture of 4% - 16% - 80% of $\text{HCl}:\text{Xe}:\text{Ne}$ respectively. Large quantities of this mixture were prepared and stored in a separate gas bottle (see Fig 22). Before starting a discharge experiment, the mercury lamp was turned on and was always allowed enough time to warm up and stabilize. The water cooling system was also turned on. Depending on what mercury spectral line was going to be used for the absorption

spectroscopy measurement, i.e., either the 3131Å or 3650Å, determined what filter was placed in front of the monochromator, and the monochromator was appropriately tuned.

With the gas valves and diffusion pump closed, the system was pumped out to ≤ 0.1 Torr with the roughing pump. Once the level of pressure was attained, the bellows valve cutting off the roughing pump from the system was closed and the diffusion pump was opened, pumping on the hollow cathode and connecting lines. The diffusion pump was left to operate until pressures on the order of 10^{-5} Torr were achieved. The diffusion pump was then closed and gas of the predetermined mix was bled into the system until the pressure needed for the experiment was obtained. When H_2 was added to the gas mix, the procedure was changed slightly. The appropriate pressure of H_2 was first bled into the system, with the standard mix then allowed to fill the system the rest of the way to the final total pressure desired. H_2 partial pressures were 0.230 and 0.460 Torr for mixes of 6 Torr total pressure and 0.160 Torr for mixes of 4 Torr total pressure. The full range experimental operating total pressures were 2, 4, and 6 Torr. The low pressures were used so as to have the negative glow of the hollow cathode extend uniformly over as much as possible of the inner diameter of the cathode tube, as explained earlier. The copper seal bellows valve was then closed, sealing the discharge tube off from the pumping station.

The lamp intensity through the gas was monitored for 30 seconds. This would allow a check at the end of the experiment to see if the lamp had changed intensity during the experiment. The lamp light was then blocked off from entering the discharge tube and the voltage from

the 3KW power supply was turned up until the gas was broken down. The current regulator was then adjusted to give the amount of current wanted for the discharge. This was monitored with the ammeter, and experimental parameters for current flow into one anode were 10, 20, 30, 40, and 50 mA. This meant total discharge currents of 100, 200, 300, 400, and 500 mA. The discharge's emission was monitored for five minutes with the counters. Later, experiment discharge runs of ten and twenty minutes were done. After the discharge emission had been monitored for the appropriate length of time, the lamp was unblocked and the lamp plus discharge emission was monitored for thirty seconds and then the lamp was blocked for another ten seconds. This was done to look for further changes in discharge intensity. At the end of the ten seconds, the lamp was unblocked and the discharge turned off. The lamp's intensity through the gas was monitored for thirty seconds. The printer was then turned off and the valve to the roughing pump would then be opened and the hollow cathode was pumped out for two minutes.

This is more than enough time to pump out the tube to pressures $< .02$ Torr. After the pump out by the roughing pump, the lamp intensity through the discharge tube would then be monitored for another 30 seconds. The ratio of the average of the counts per second of the lamp intensity through the gas to the average of the counts per second of the intensity through the pumped out tube is used in determining the fraction of absorption by Cl_2 .

When monitoring the XeCl^* 308 nm emission, the procedure of filling the system with the gas mixes (either the standard mix or the standard mix with H_2 added) was the same as described above. In

monitoring the emission of the XeCl^* discharge, no filter was used and the tube was sealed off from any other forms of light.

IV. Results

From Fig 3, it can be seen that Cl₂ absorbs strongly in the 300 to 400 nm wavelength region. The mercury lamp has two strong spectral emission lines in that region, the 3131Å and 3650Å lines. These two lines were used in the U.V. photoabsorption spectroscopy experiments of the thesis. Ne, Xe, HCl, and XeCl do not absorb these lines. The mercury lamp radiation was passed through the gas immediately after a discharge was run and the counts were measured of the photons of either the 3131Å or 3650Å lines, depending on which line was used in the experiment. This measurement would give the intensity (I) of the radiation making it through the gas after absorption by Cl₂ in the discharge. It was assumed that once the discharge was shut off, the Cl₂ concentration was constant while the photon counting was taking place. The tube would then be pumped out and the intensity of the light source would be measured (I₀). The expression used for evaluating the partial pressure of Cl₂ when using the 3131Å line was:

$$\frac{-T_{Cl_2}}{65.615} \ln \frac{I}{I_0} = P_{Cl_2} \quad (62)$$

where

T_{Cl₂} = Temperature of the Cl₂ gas in °K

P_{Cl₂} = Partial pressure of Cl₂ in Torr

The expression for evaluating the partial pressure of Cl₂ when the 3650Å line was used is quite similar:

$$\frac{-T_{Cl_2}}{35.167} \ln \frac{I}{I_0} = P_{Cl_2} \quad (63)$$

Appendix A contains the derivation of these expressions.

For a value of T_{Cl_2} , the temperature of the cathode's wall was used for the temperature of the gas species. This was reasoned due to the low pressures (≤ 6 Torr) in the discharge tube, allowing the gas and wall of the discharge tube to equilibrate rapidly (Ref 18). See Appendix B for a derivation of the equation used for the calculation of the standard deviation of error for Eqs (62) and (63).

The original experimental parameters were to use the premixed gas of HCl/Xe/Ne in 4%/16%/80% mix ratio at pressures of 2, 4, and 6 Torr. For each pressure, the total discharge current was to be set at 100, 200, and 400 mA. The $3131\overset{\circ}{\text{Å}}$ line was to be used for the experiment. The values of the partial pressures of Cl_2 from these experiment runs was quite erratic and at low pressures and current, the partial pressure results were lost in the standard deviation of error. It was felt that at low pressure and current the Cl_2 concentration was too small for the system to measure and the erratic behavior of the other results was due to photons from the strong 308 nm band of $XeCl^*$ being passed through the system. It was then decided to use the $3650\overset{\circ}{\text{Å}}$ line for the absorption spectroscopy. In addition, the experimental parameters were narrowed down to just mix pressures of 4 and 6 Torr and total currents of 200, 300, 400, and 500 mA.

Table IV gives the data taken using the $3650\overset{\circ}{\text{Å}}$ line and five minute discharge runs. It also emphasizes some problems that were encountered in the experiment. The data is fairly scattered, due to four main reasons:

Table IV
Data for 5 Minute Runs Using 3650Å Line

Run No.	Pressure (Torr)	Current (mA)	Pressure Cl ₂ (Torr)	Error (±Torr)	T °K
1	6.004	200	0.1061	0.0406	296.15
2	4.002	400	0.1125	0.0225	296.65
3	6.004	400	0.1263	0.0207	296.65
4	4.003	200	0.0459	0.0285	295.15
5	6.004	200	0.0808	0.0227	295.15
6	4.002	300	0.0738	0.0252	295.15
7	6.003	300	0.0643	0.0296	297.15
8	4.002	500	0.0822	0.0343	296.15
9	6.004	500	0.0168	0.0184	296.65
10	6.011	200	0.0085	0.0312	296.65
11	6.011	300	0.0700	0.0259	296.65
12	6.005	500	0.0722	0.0262	297.15
13	4.002	500	0.1478	0.0155	297.15
14	6.002	200	0.0129	0.0341	295.65
15	6.001	400	0.0559	0.0205	296.15
16	6.002	400	0.0284	0.0324	296.15
17	6.002	500	0.0966	0.0550	296.15
18	6.002	200	0.0243	0.0326	295.65
19	6.003	400	0.1135	0.0235	295.65
20	6.002	500	0.1267	0.0203	296.15
21	6.003	500	0.0495	0.0201	295.15
22	6.003	400	0.0116	0.0535	295.15
23	6.006	300	0.0402	0.0248	295.15
24	6.006	200	0.0261	0.0259	295.15
25	6.003	300	0.0886	0.0408	295.65
26	6.003	400	0.1169	0.0252	296.15
27	6.003	500	0.1913	0.0255	295.65

1. The PMT saturated at counts $\sim 1.2 \times 10^6$. Therefore, the greatest accuracy that could be achieved by the experiment was:

$$\sigma = \sqrt{1.2 \times 10^6} = 1.1 \times 10^3$$

or three significant figures. This was barely sensitive enough to measure Cl_2 absorption.

2. The availability of only one PMT for counting meant another one could not be used to monitor fluctuations in the mercury source during the absorption measuring.

3. After several runs had been made, a deposit of a yellow-brownish material was observed to form on the windows. This would cause the intensity of the lamp before the run was made to be greater than the intensity after the run and pump out. The windows were taken off and cleaned. The assumption was made that after the discharge was shut off, the material would stop forming on the windows and be a constant absorber during the measurements.

4. In experiments run by G. Vogel taking spectra of gas discharges in the HCD, he noticed Cl_2 spectra even after pump out of just Xe-Ne discharges.

Figure 26 shows the partial pressures of Cl_2 found for varying currents and a total gas mix pressure of 4 Torr. Figure 27 shows the results for the 6Torr total pressure case. The data points and error bars shown are calculated using a weighted averaging and standard deviation technique (Ref 77). The error bars are for error in the intensity of the lamp and error in the temperature measurement. The theoretical limit is defined as one half of the partial pressure of HCl initially in the mix. This limit is defined as the total amount of Cl_2 that could be formed due to just the HCl of the mix, i.e., if all the HCl dissociated and its Cl all recombined to form Cl_2 .

In both Figs 26 and 27, the Cl_2 concentration increases with increasing current. The 4 Torr case reaches the maximum theoretical

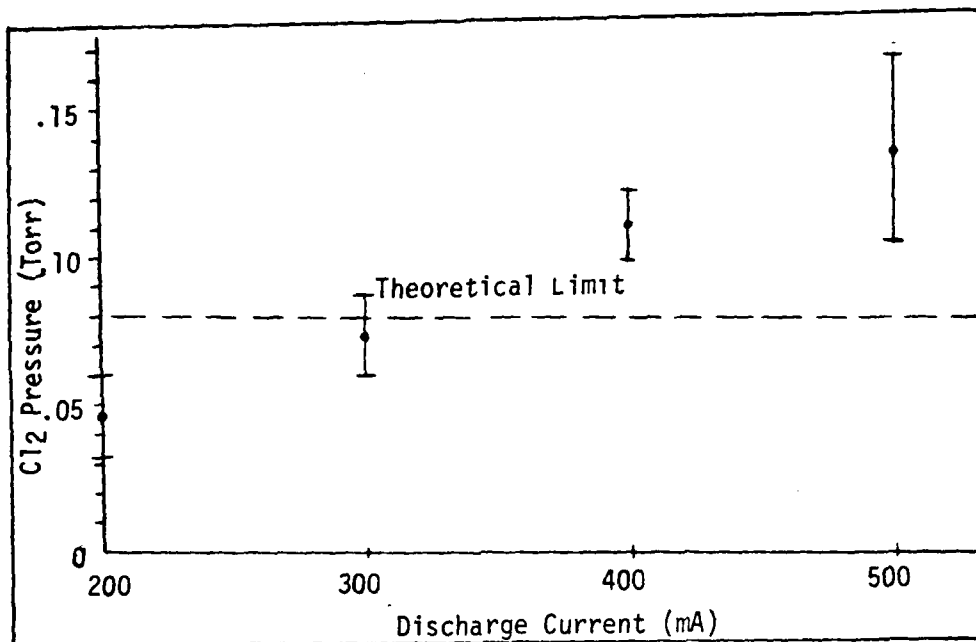


Fig 26. Partial Pressure of Cl₂ vs Current
for a Total Gas Pressure = 4 Torr

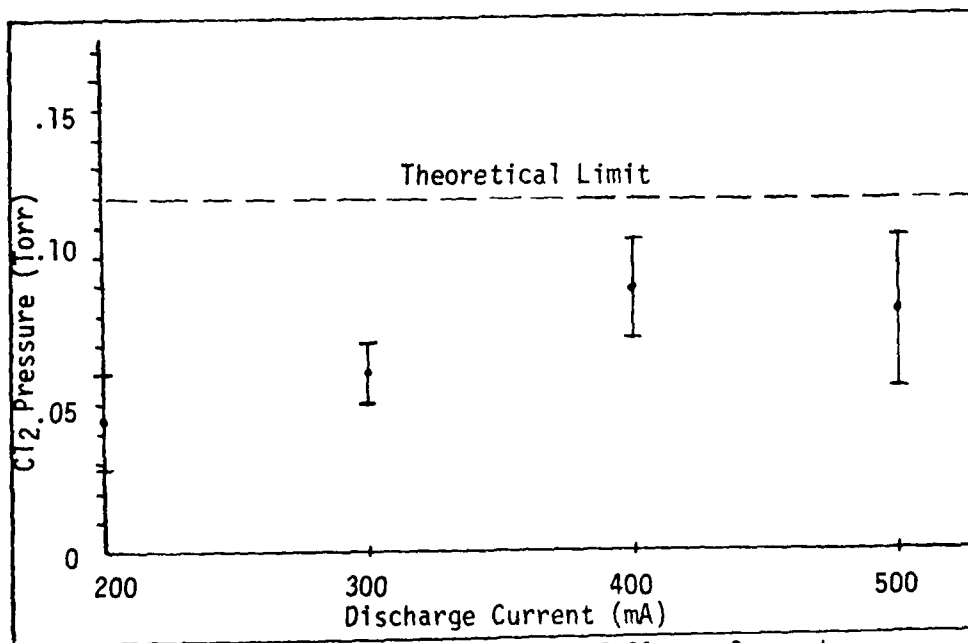


Fig 27. Partial Pressure of Cl₂ vs Current
for a Total Gas Pressure = 6 Torr

limit of Cl_2 partial pressure at total discharge currents just greater than 300 mA and exceeds the theoretical limit at higher currents. The 4 Torr case also allows a greater amount of Cl_2 at 200 mA than does the 6 Torr case. The 6 Torr total pressure plot shows the Cl_2 partial pressure increasing from 200 to 300 mA and saturates at a level that is much lower than the theoretical limit partial pressure. At higher currents, the Cl_2 partial pressure even seems to lower for the 6 Torr case.

H_2 was then added to the mix to see if any change in the Cl_2 concentration could be observed. As stated before, it was hoped that the addition of H_2 would cause Eq (26) to produce more HCl by reacting with the Cl_2 (Ref 6). The H_2 partial pressure of 0.23 Torr is nearly twice the theoretical limit of Cl_2 possible in the discharge for a 6 Torr gas mix. Figure 28 shows the resulting data points. The data for the 0.230 Torr partial pressure of H_2 was fairly erratic and nothing could be concluded from it. The 0.460 Torr partial pressure of H_2 did seem to lower the Cl_2 concentration, but not by as dramatic an amount as would be expected from such a large amount of H_2 .

The results of the experiments performed by McKee (Ref 6) show that longer and stable high pressure XeCl^* laser emission is attained when H_2 is added than when H_2 is not. Their experiment was run at total pressures greater than 2000 Torr and used a U.V. preionization transverse-electric field discharge. It was decided to observe the XeCl^* 308 nm emission of a 6 Torr total pressure mix in the HCD and compare it to XeCl^* emission with 0.230 Torr and 0.460 Torr of H_2 within the standard mix at a 6 Torr total pressure. The discharge

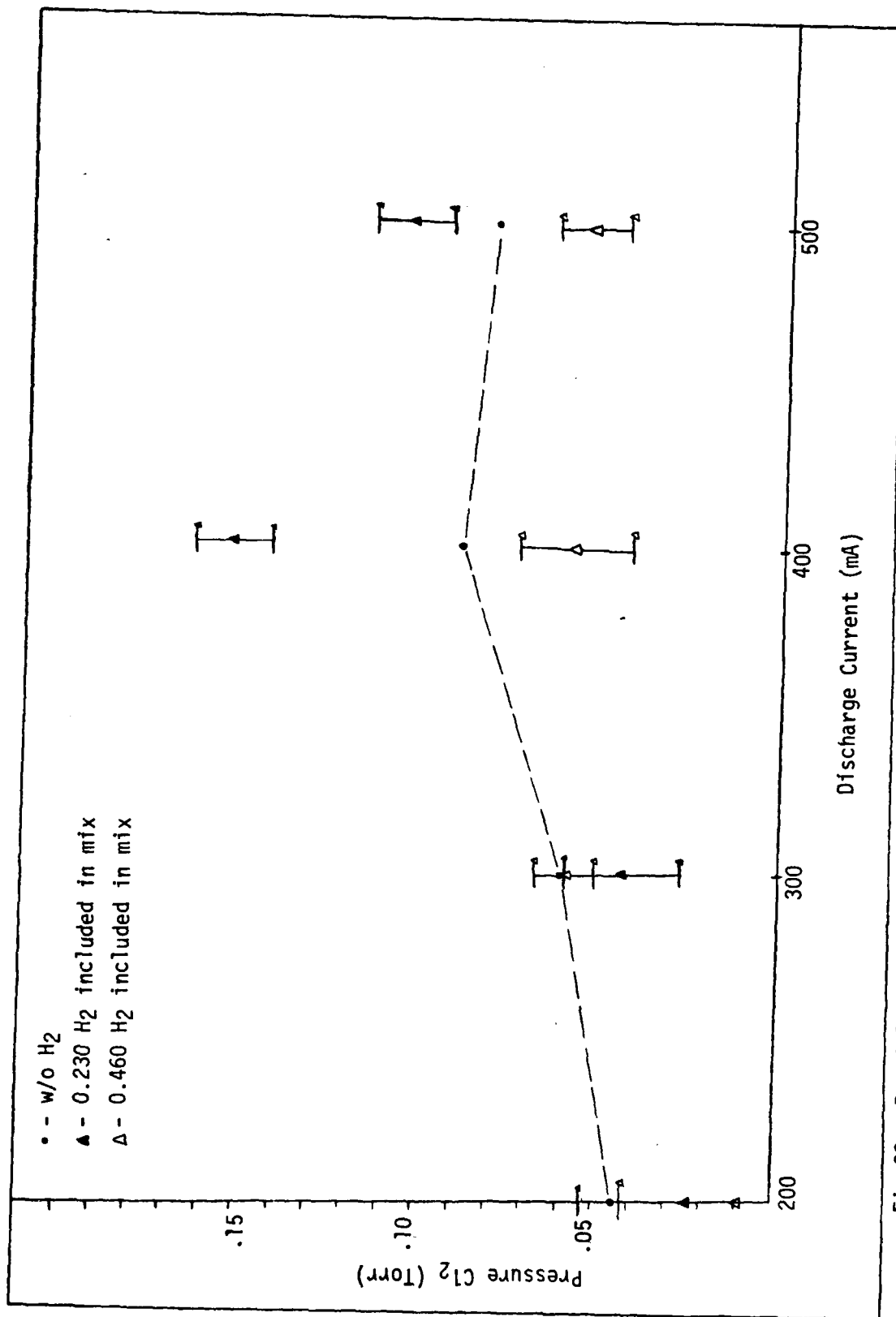


Fig 28. Partial Pressure of Cl_2 with 0.230 and 0.460 Torr of H_2 included with a 6 Torr Total Gas Pressure

was run for 10 minutes. Figure 29 shows the various photon counts versus time plots for the XeCl* 308 nm emission without H₂ addition. Figure 30 shows the XeCl* emission with 0.230 Torr of H₂ added. Note the lowering and stabilization of the intensity. The addition of 0.460 Torr of H₂, as seen in Fig 31, has the same stabilizing effect at approximately the same values as the 0.230 Torr H₂ addition cases. A rise in the emission with 0.460 Torr H₂ added is seen as time progressed for the 300, 400, and 500 mA cases; however, the emissions with the H₂ added never seemed to go above the lowest level of XeCl* emission measured without H₂ additives. The 6 Torr plots seem to contradict results of McKee. One would expect to observe a value of XeCl* emission with H₂ additive in the mix to be much higher than the leveling value of the XeCl* emission without the H₂, if not the initial emission value. Table V shows how the discharge voltage varied with different H₂ partial pressures added to the mix. As can be seen, the more H₂ added to the mix, the higher the discharge voltage.

Table V

Variations in Discharge Voltage with and without H₂ Additions

Pressure	200 mA	300 mA	400 mA	500 mA
6 Torr .04/.16/.80	308	317	324	328
6 Torr inc. 23T. H ₂	361	375	386	393
6 Torr inc. 46T. H ₂	365	381	394	408
4 Torr .04/.16/.80	338	347	352	357

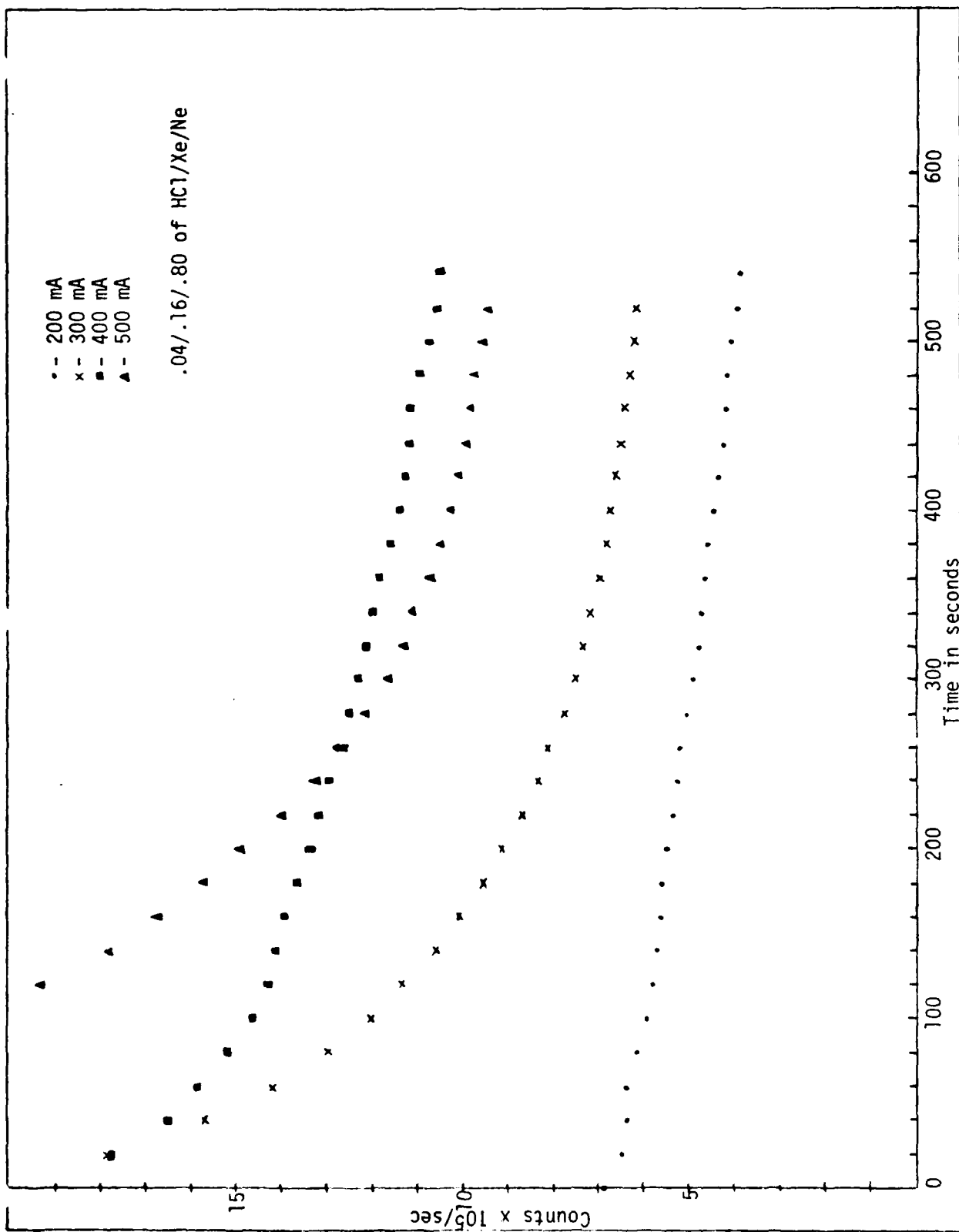


Fig 29. XeCl* 308 nm Emission versus Time and Discharge Current at 6 Torr

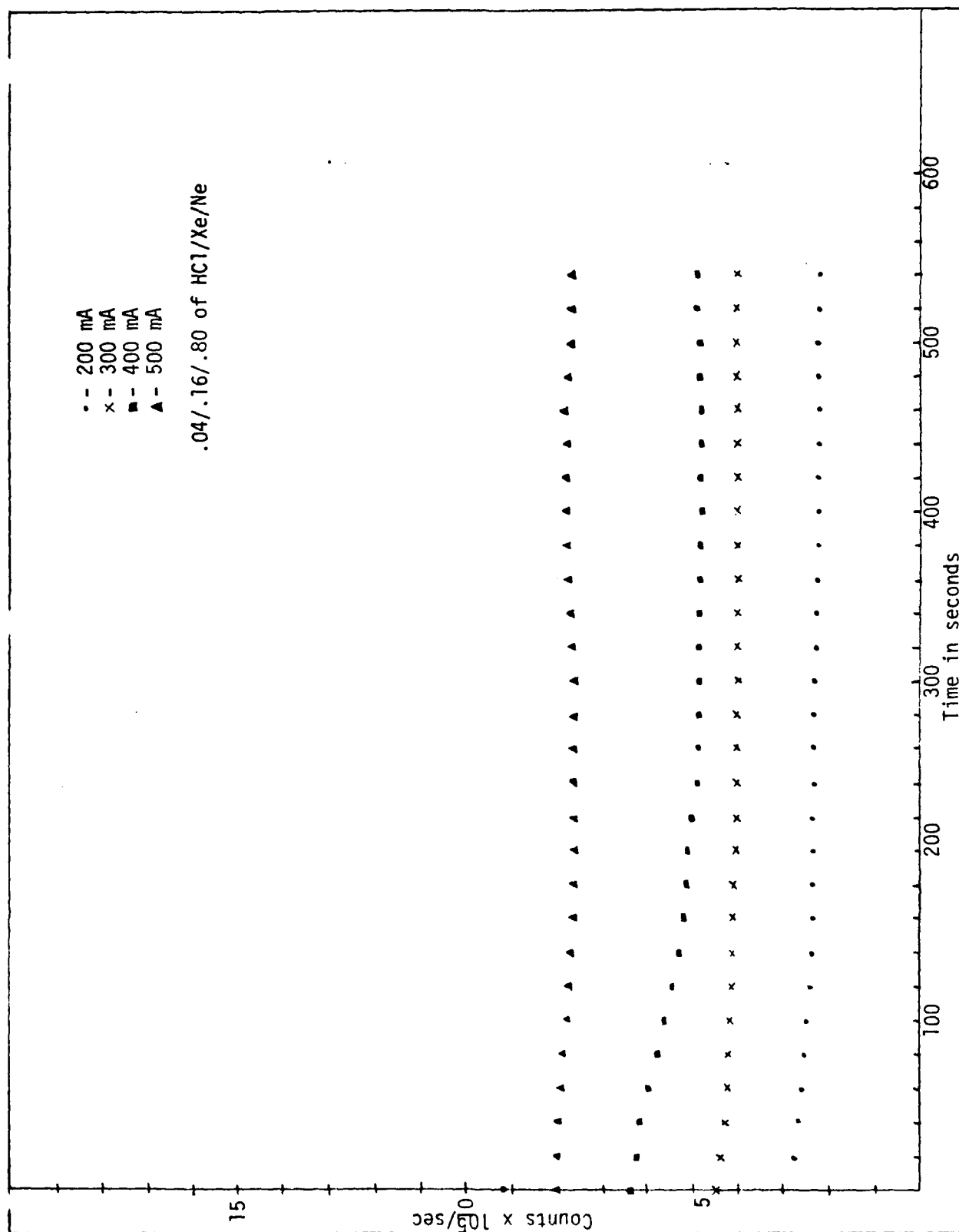


Fig 30. XeCl* 308 nm Emission with 0.230 Torr Partial Pressure of H₂ versus Time and Discharge Current at 6 Torr

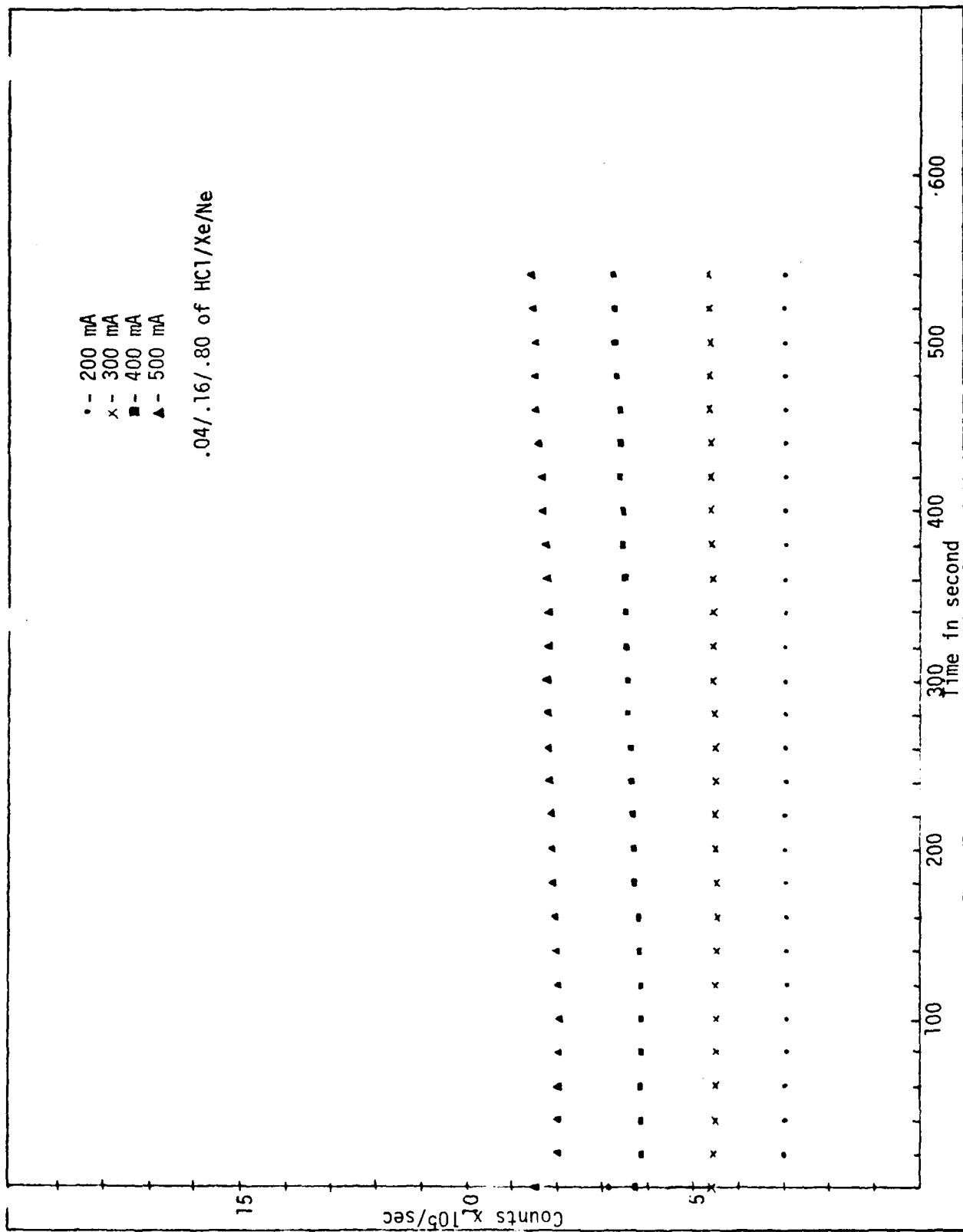


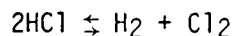
Fig 31. XeCl* 308 nm Emission with 0.460 Torr Partial Pressure of H₂ versus Time and Discharge Current at 6 Torr

V. Conclusions

In order to provide a framework for establishing the implications of the experimental observations, a brief review of these results is in order. The measurements can be divided into two cases, case A in which the source of H_2 was only the initial HCl concentration within the mix, the second, case B, when concentrations of H_2 were deliberately added to the discharge mix. In both cases, measurements were made of the Cl_2 concentration versus current at total gas pressures of 4 and 6 Torr, and the $XeCl^*$ 308 nm spontaneous emission versus time.

In case A, the Cl_2 concentration increased with increasing current for both the 4 and 6 Torr pressure runs, as shown in Figs 26 and 27. The Cl_2 concentration saturated at a total current of 400 mA for the 6 Torr case. In the 4 Torr case, a similar increase of Cl_2 is observed, but at currents greater than 400 mA, the concentration of Cl_2 exceeded that which could originate from the original 0.16 Torr of HCl . The $XeCl^*$ emission monitored at 308 nm decreased with discharge run time for all the total current runs (Fig 29).

In case B, the addition of H_2 to the gas mix had no significant effect on the observed concentration of Cl_2 , i.e., H_2 addition did not force the reaction



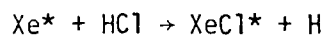
to the left, forming more HCl and depleting the Cl_2 concentration. The $XeCl^*$ 308 nm emission stabilized with the addition of H_2 to the gas mix, but the intensity was lower than the final measured intensity of the $XeCl^*$ emission without H_2 added. This was true for all current

runs. When twice as much H₂ as what was originally added was added to the mix, there was no significant change in the intensity of the XeCl* emission as compared with the emission with the original H₂ addition.

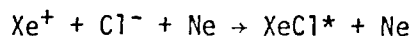
The primary formation channel of XeCl* was assumed to be:



because of the low branching ratios at low pressures for the reaction (Refs 11 and 14):



The ion reaction:



was also not considered to be a major formation channel because three body reactions are more efficient at high pressure, and the experiments with the HCD were conducted at low pressures.

Let us first address the increase of the Cl₂ concentration with increases in discharge current. As the current increased, the electron number density increases causing more dissociation of HCl and more dissociative attachment between the electrons and Cl, giving Cl⁻. The Cl⁻ undergoes reactions in the discharge that allow the formation of Cl₂. This explains the increase in Cl₂ concentration, but why is there such a large increase, even increasing past the theoretical limit in the 4 Torr case? It is possible that the greater currents in the discharge result in the release of adsorbed Cl on the discharge

tube's walls, which can recombine with another Cl and form Cl₂. This hypothesis is substantiated by looking at spectra from the HCD. It was found by Vogel (Ref 7) that if a pure Xe discharge was run after a discharge was run containing HCl in the mix, XeCl* emission could still be observed. Therefore, Cl₂ concentrations greater than what can be achieved by the gas mix itself are possible.

In order to understand the observed decrease in the XeCl* emission, both Cl⁻ and Cl₂ are considered as possible dominant 308 nm radiation absorbers in the HCD. First, the possibility that Cl⁻ is the dominant absorber will be discussed. As presented earlier, Cl⁻ has a 308 nm photon absorption cross section a hundred times greater than Cl₂ ($2.2 \times 10^{-17} \text{ cm}^2$ for Cl⁻ and $1.7 \times 10^{-19} \text{ cm}^2$ for Cl₂). For the Cl⁻ to be as significant an absorber as the Cl₂, the number density of Cl⁻ would have to be at least 1% of the Cl₂ number density. Normally, negative ion concentrations in glow discharges are quite small, due to diffusion losses. By looking at the current density expression and negative ion production rate equation, it will be possible to determine if such appreciable quantities of Cl⁻ can exist in the HCD. The current density j is given by:

$$j = n_e \mu_e e E + n_- \mu_- e E + n_+ \mu_+ e E \quad (64)$$

where

n_e, n_-, n_+ = number density of the electrons, negative ions and positive ions. cm^{-3}

μ_e, μ_-, μ_+ = mobilities of the electrons, negative ions and positive ions. $\text{cm}^2 \text{V}^{-1} \text{s}^{-1}$

$e = 1.6 \times 10^{-19}$ coulombs, electronic charge

E = electric field. V-cm^{-1}

We wish to get an upper bound on the Cl^- concentration. If we assume that the current is carried by the Cl^- ions alone, and the $n_- = n_+$ and $\mu_- = \mu_+$, we find:

$$n_- = \frac{j}{2\mu_- eE} \quad (65)$$

Using the 400 mA 6 Torr runs as an example, the current density would be:

$$j = \frac{40 \times 10^{-3} \text{ Amps}}{\pi(0.3875 \text{ cm}^2)} = 0.0848 \text{ Amps} \cdot \text{cm}^{-2} \quad (66)$$

where 40 mA is the current flowing into one of the ten anodes and 0.3875 cm^2 is the radius of the discharge tube. The voltage across the tube was 324V (from Table V), and with the diameter of the tube being 0.775 cm, a value for the electric field is obtained

$$E = \frac{324\text{V}}{0.775 \text{ cm}} = 418.06 \text{ V} \cdot \text{cm}^{-1} \quad (67)$$

Assuming that the mobility of the Cl^- negative ions is approximately the same as the mobility of the positive ions in a Ne gas, a value of $8.2 \text{ cm}^2 \text{ V}^{-1} \text{ s}^{-1}$ is obtained (Ref 78). Substituting these values back into Eq (65), one finds the number density of Cl^- :

$$n_- = 7.73 \times 10^{13} \text{ cm}^{-3} \quad (68)$$

The maximum number density of Cl_2 possible from the amount of HCl present in the 6 Torr runs is $4.26 \times 10^{15} \text{ cm}^{-3}$. The value found above for Cl^- is 1.8% of the maximum Cl_2 number density. Thus, at this point, Cl^- appears to be a possibility as a major absorber. To

establish the consistency of the assumed dominance of n_- over n_e , we now consider the negative ion production equation.

The time rate of change of the negative ion concentration, \dot{n}_- , is given by:

$$\dot{n}_- = kN_A n_e - \alpha n_-^2 \quad (69)$$

where

k = rate constant of negative ion production. $\text{cm}^3\text{-S}^{-1}$

N_A = number density of electron attaching species, HCl or Cl_2 . cm^{-3}

α = ion recombination rate constant. $\text{cm}^3\text{-S}^{-1}$

Assuming steady state condition and solving for n_e , we find:

$$n_e = \frac{\alpha n_-^2}{kN_A} \quad (70)$$

The values for α and k for the Cl^- ions could not be found, but values from comparable reactions should suffice. When the values of $\alpha = 2 \times 10^{-6} \text{ cm}^3 \text{-S}^{-1}$ (Ref 58), $k = 4 \times 10^{-10} \text{ cm}^3 \text{-S}^{-1}$ (Ref 58), the Cl^- concentration previously calculated, and letting N_A equal to the initial number density of HCl of the mix ($8.5 \times 10^{15} \text{ cm}^{-3}$), are substituted back in Eq (70) we find an electron number density of $3.51 \times 10^{15} \text{ cm}^{-3}$. This value of an electron number density is greater than the value of n_- that was calculated. Since the mobility of electron is larger than the mobility of ions, the majority of the current, under the conditions we have specified, will be carried by the electrons. Thus our previous assumptions are false and we conclude that Cl_2 is the dominant absorber of $\text{XeCl}^* 308 \text{ nm}$ emission in the HCD.

To explain the effect of Cl_2 absorption of XeCl^* emission, it should be recalled that as the discharge current was increased, the observed Cl_2 concentration also increased. This increase of Cl_2 with increases of current was due to more dissociative attachment occurring and more absorbed Cl being released from the walls of the discharge going to form Cl_2 . Since the total amount of Cl coming off the walls increased with increasing current, a reasonable assumption is that the total amount of Cl that comes off the walls increases with time also. This increase of Cl allows more Cl_2 to be formed and allows more XeCl^* to form, as seen on Fig 29 by the emission of XeCl^* at the higher current as compared to the emission at lower currents. The increase in Cl_2 also means more Cl_2 to absorb the 308 nm radiation. The effect of more Cl_2 for absorption is seen in Fig 29 by the greater drops, in general, of the intensity of the XeCl^* emission as the current is increased.

When H_2 was deliberately added to the discharge, there was no great reduction in the Cl_2 concentration (see Fig 28). It must be remembered that the Cl_2 concentration measurements were made with the discharge off. This non-reactive condition allows time for the Cl_2 to equilibrate with the walls.

The lowering in XeCl^* intensity of emission when H_2 is added (see Figs 30 and 31) can be explained as follows. It is postulated that H_2 causes the rapid desorption of Cl from the walls of the discharge. This is a good assumption since it was found that after discharges of pure H_2 were run, Cl_2 was still being detected in significant quantities. This effect seems to be so efficient that

the discharge is swamped with Cl. The additional amounts of Cl increases the Cl₂ concentration. The large concentration of Cl₂ allows the formation of XeCl* to occur as fast as Xe* metastables are formed, accounting for the stability of the emission. However, the large background Cl₂ concentration also absorbs the emission, lowering the output intensity that was monitored. It appears that relatively small amounts of H₂ addition to the gas mix is quite effective in clearing the walls of Cl, for when greater amounts of H₂ were added to the mix, the XeCl* emission intensity hardly changed (compare Figs 30 and 31).

There are three main conclusions to be drawn from the experiments:

1. Cl is absorbed in the walls of the discharge tube and returned to the gas under discharge conditions. The rate of return increases with current.
2. H₂ is quite effective in clearing the Cl off the discharge walls.
3. Cl₂ appears to be the dominant XeCl* 308 nm emission absorber.

The Recommendations chapter will propose experiments that can provide data to help in the further understanding of a XeCl hollow cathode discharge.

VI. Recommendations

Several proposals for future study with a XeCl discharge in a hollow cathode are recommended. A repeat of the thesis experiment only utilizing two PMTs, one for measuring the absorption of the lamp source's light and another for monitoring the lamp's output intensity. Another recommendation would be to obtain a lamp source with a higher intensity in the 300-400 nm spectral range. Both of these suggestions are made so as to increase the accuracy of the experiment.

A broad band U.V. spectroscopy experiment might be done to look at variations in the intensity of the spectral emissions from the discharge. The variation of the Cl₂ concentration in the discharge with time would prove to be a most enlightening experiment. These experiments would help in the determination of the reaction kinetics involved. A spectroscopic experiment to find out what was being deposited on the windows of the discharge tube would also be interesting. An experiment using the same procedure as used in the thesis experiment only monitoring the HCl concentration could be conducted. More experiments involved with monitoring the XeCl* 308 nm emission intensity with the addition of H₂ or other additives to the XeCl discharge mix are highly recommended.

Bibliography

1. Ewing, J. J. Physics Today., 31:32 (1978).
2. Eden, G., Burnham, R., Champagne, L. F., Donohue, T., and Djeu, N. IEEE Spectrum. Page 50 (April 1979).
3. Pedrotti, L. Lecture Materials distributed in PH 7.43, School of Engineering, Air Force Institute of Technology, Wright-Patterson AFB, Ohio, 1980.
4. Alberti, F. OSA Handbook of Optics. 8-34 (Fig 14). Edited by W. G. Driscoll.
5. Rothe, D. E., West, J. B., Bhaumik. IEEE J. Quant. Electron., 15: 314 (1979).
6. McKee, T. J., James, D. J., Nip, W. S., Weeks, R. W., and Willis, C. Applied Phys. Lett., 36: 943 (1980).
7. Vogel, G. AFIT Thesis on Hollow Cathode Discharge of XeCl (in preparation).
8. Ginter, M. L., Battino, R. J. Chem Phys., 52: 4469 (1970).
9. Fitzsimmons, W. A. Atomic Physics 3. Edited by S. J. Smith and G. K. Walters. New York: Plenum Press, 1973.
10. Hay, P. J. and Dunning, T. H. J. Chem. Phys., 69: 2209 (1978).
11. Brashears, H. C., Jr., and Setser, D. W. J. Phys. Chem., 84: 224 (1980).
12. Tamagake, K., Kolts, J. H., and Setser, D. W. J. Chem. Phys., 71: 1264 (1979).
13. Tellinghuisen, J., Hoffman, J. M., Tisone, G. C., Hays, A. K. J. Chem. Phys., 64: 2484 (1976).
14. Kolts, J. H., Velazco, J. E., and Setser, D. W. J. Chem. Phys., 71: 1247 (1979).
15. Ewing, J. J. and Brau, C. A. Phys. Rev. A., 12: 129 (1975).
16. Dunning, T. H., Jr. and Hay, P. J. Appl. Phys. Lett., 28: 649 (1976).
17. Hay, P. J. and Dunning, T. H., Jr. J. Chem. Phys., 66: 1306 (1977).
18. DeJoseph, Charles. Wright Aeronautical Laboratory, Plasma Physics Branch (private communication).

19. Lorents, D. C., Heustis, D. L., McCusken, M. V., Nakano, H. H., and Hill, R. M. J. Chem. Phys., 68: 4657 (1978).
20. Fisher, C. H., Center, R. E., and McDaniel, J. P. Paper AB-3, presented at the 32nd Gaseous Electronics Conference, Pittsburgh, Penn., (October 1979).
21. Ewing, J. J. and Brau, C. A. Appl. Phys. Lett., 27: 350 (1975).
22. Bardsley, J. N. and Biondi, M. A. Advances in Atomic and Molecular Physics. New York: Academic Press, 1970.
23. Gundel, L. A., Setser, D. W., Clyne, M. A. A., Coxon, J. A. and Nip, W. J. Chem. Phys., 64: 4390 (1976).
24. Gedanken, A. G., Jortner, J., Raz, B., and Szoke, A. J. Chem. Phys. 57: 3456 (1972).
25. Caledonia, G. E. Chem. Rev., 75: 333 (1975).
26. Christophorou, L. G. Atomic and Molecular Radiation Physics. London: Wiley and Sons, 1971.
27. Chen, J. L., Center, R. E., Trainor, D. W., and Fyfe, W. I. Appl. Phys. Lett., 30: 99 (1977).
28. Nygaard, K. J., Hunter, S. R., Fletcher, J., and Foltyn, S. R. Appl. Phys. Lett., 32: 351 (1978).
29. Johnson, T. H. and Hunter, A. M., II. J. Appl. Phys., 51: 2406 (1980).
30. Velazco, J. E., Kolts, J. H., and Setser, D. W. J. Chem. Phys., 65: 3468 (1976).
31. Thompson, J. J. Philos. Mag., 47: 337 (1924).
32. Langevin, P. Ann. Chem. Phys., 28: 433 (1903).
33. Mangano, J. A., Jacob, J. H., Rokni, M., and Hawryluk, A. Appl. Phys. Lett., 31: 26 (1977).
34. Setser, D. W. Seventh Winter Colloquium on High Power Visible Lasers, Park City, Utah (1977) and subsequent private communication to Ch. A. Brau. Quenching of KrF* by Xe was observed to be very fast (of the order of gas kinetic), but XeF* emission was very weak.
35. Lorents, D. C. Physica, 82c: 19 (1976).
36. Brau, C. A. Appl. Phys. Lett., 29: 7 (1976).
37. Rokni, M., Jacob, J. H., Managano, J. A., and Brocha, R. Appl. Phys. Lett., 31: 79 (1977).

38. Tang, K. Y., Lorents, D. C., and Huestis, D. L. Paper AB-5, presented at the 32nd Gaseous Electronics Conference, Pittsburgh, Penn (October 1979).
39. ---- Laser Meeting, Williamsburg, Virginia. August 1979.
40. Waynant and Eden, G. Appl. Phys. Lett., (February 1980).
41. Seery, D. J. and Britton, D. J. Phys. Chem., 69: 2263 (1964).
42. Rothe, D. E. Phys. Rev., 177: 93 (1969).
43. Lorents, D. C., et al. SRI Rpt. MP73-2, Stanford Res. Inst. Unpublished Text. Menlo Park, California, 1973.
44. Gibson, G. E. and Bayless, N. S. Phys. Rev., 44: 188 (1933).
45. Wadt, W., et al. Appl. Phys. Lett., 31: 672 (1977).
46. Phelps, A. V. and Molnar, J. P. Phys. Rev., 82: 1202 (1953).
47. Gaur, J. P. and Chanin, L. M. Phys. Rev., 182: 167 (1969).
48. Kasner, W. H. Phys. Rev., 164: 194 (1967).
49. Leichner, P. K., et al. Phys. Rev. A., 13: 1787 (1976).
50. Vitois, A. P. and Oskam, H. J. Phys. Rev. A., 8: 1860 (1973).
51. Bardsley, J. N. and Biondi, M. A. Adv. At. Mol. Phys., 6: 2 (1970).
52. Bourene, M. and LeCalve, J. J. Chem. Phys., 58: 1452 (1973).
53. Gleason, R. E., et al. J. Chem. Phys., 66: 1589 (1977).
54. Bohme, D. K., et al. J. Chem. Phys., 52: 5094 (1970).
55. Chen, C. L. Phys. Rev., 131: 2250 (1963).
56. Rice, J. K., Johnson, A. W. J. Chem. Phys. 63: 5238 (1975).
57. von Engel, A. Ionized Gases, 2nd ed., Great Britain: Oxford University Press, 1965.
58. Rhodes, Ch. K., Editor. Topics in Applied Physics. Volume 30. Berlin and Heidelberg: Springer-Verlag, 1979.
59. Gill, P. and Webb, C. E. J. Phys. D: Appl. Phys., 10: 299 (1977).

60. Crane, J. K. and Verdeyen, J. T. J. Appl. Phys., 51: 123- (1980).
61. Schuebel, W. K. Proc. XI Int. Conf. Phenomena in Ionized (Czech. Academy of Science, Prague, Czech., 1973).
62. Janossy, M., Csillag, L., Rozsa, K., and Salamon, T. Phys. A, 68: 317 (1978).
63. Janossy, M., Rozsa, K., Csillag, L., and Bergow, J. Phys. A, 46: 379 (1974).
64. Rozsa, K., Janossy, M., Bergow, J., and Csillag, L. Opt. C 23: 15 (1977).
65. Nuchkov, N. K., Grozeva, M. G., and Sabotinov, N. V. Opt. 27: 114 (1978).
66. Pacheva, Y., Stefanova, M., and Pramatarov, P. Opt. Commun 121 (1978).
67. Verdeyen, J. T., Cherrington, B. E., Griffin, S. T., and Si M. H. Progress Report P-12528-P. Presented at Gaseous Electron Conference, Palo Alto, CA, October 1977.
68. Bailey, W. F. Lecture materials distributed in PH 7.51, School of Engineering, Air Force Institute of Technology, Wright-Patterson AFB, Ohio, 1980.
69. Penning, F. M. Handout in PH 7.51, School of Engineering, Force Institute of Technology, Wright-Patterson AFB, Ohio, 1980.
70. Borodin, V. S. and Kagan, Yu M. Sov. Phys. Tech. Phys., 11: 131 (1966).
71. Gill, P. D. Phil. Thesis. University of Oxford (1975).
72. ---- Princeton Applied Research Photon Counting. Princeton New Jersey: Princeton Applied Research Corporation, 1975.
73. ---- EMI Photomultiplier Tubes, Brochure Ref: P001/fP70 by EMI Electronics Ltd. Crawley Sussex England: Bookprint Limited
74. Morton, G. A. Applied Optics, 7: 1 (1968).
75. Hengehold, R. L. Lecture materials distributed in PH 6.42, School of Engineering, Air Force Institute of Technology, Wright Patterson AFB, Ohio, 1980.
76. Solid State Radiations, Inc. Tech. Publ. 1100-1 (1969) Los Angeles, California.

77. Bevington, Philip R. Data Reduction and Error Analysis for Physical Sciences. New York: McGraw-Hill Book Company, 1969.
78. Chanin, L. M. and Biondi, M. A. Phys. Rev., 107: 1219 (1964).
79. Seery, D. J., and Britton, D. J. Phys. Chem., 68: 2263 (1964).

Appendix A

This appendix deals with the derivation of the equations to determine the partial pressures of Cl_2 .

The relationship between I and I_0 is Beer's Law from Eq

$$I = I_0 e^{-n\sigma x}$$

The σ is related to the extinction coefficient by:

$$\sigma = \frac{c\Lambda_a}{n}$$

where

Λ_a = extinction coefficient in $\text{l mol}^{-1} \text{cm}^{-1}$

c = number of mol l^{-1}

Table VI lists the extinction coefficients for Cl_2 in the spectral region of interest (Ref 79). The Λ_a for the 3131\AA and 3650\AA were linearly interpolated and found to be 52.4 and 28.10 $\text{l mol}^{-1} \text{cm}^{-1}$ respectively. The cross section is expected to have a small variation on pressure and was assumed to be the same as the cross section Cl_2 would have at STP. Using STP conditions, Eq (A1) becomes letting $n = 2.6872 \times 10^{19} \text{ cm}^{-3}$ (Loschmidt's number), and $c = (22.4 \frac{\text{l}}{\text{mol}})^{-1}$:

$$\sigma = 1.6613 \times 10^{-21} \cdot \Lambda_a$$

For 3131\AA and 1650\AA lines, their σ 's were 8.7052×10^{-20} and $4.6683 \times 10^{-20} \text{ cm}^2$ respectively.

It was desired to present the results in partial pressure rather than its number density. The derivation for this follows

AD-A094 404

AIR FORCE INST OF TECH WRIGHT-PATTERSON AFB OH SCHOOL--ETC F/G 7/4
MEASUREMENT OF CL2 CONCENTRATION IN A XECL HOLLOW CATHODE DISCH--ETC(U)
DEC 80 J D WINEGARDEN
AFIT/6EP/PH/80-12

NL

UNCLASSIFIED

2 of 2
AD-A094 404



END

DATE

FILED

2-81

DTIC

Table VI
Extinction Coefficients of Cl₂

λ (nm)	ϵ_a l mol ⁻¹ cm ⁻¹
300	31.4
310	48.3
320	61.8
330	67.0
340	61.8
350	49.6
360	34.4
370	21.8

The number density n of Cl₂ is determined by:

$$n = n_0 \frac{T_0 P_{Cl_2}}{T_{Cl_2} P_0} \quad (A3)$$

where

$$T_0 = 273.15^\circ K$$

$$P_0 = 760 \text{ Torr}$$

$$P_{Cl_2} = \text{partial pressure of Cl}_2$$

$$T_{Cl_2} = \text{temperature of Cl}_2$$

- Substituting in the values of n_0 , T_0 , P_0 , Eq (A3) reduces to:

$$n = 9.658 \times 10^{18} \frac{P_{Cl_2}}{T_{Cl_2}} \quad (A4)$$

Multiplying both sides of Eq (A4) by αx :

$$n\sigma x = 9.658 \times 10^{18} \frac{P_{Cl_2}}{T_{Cl_2}} \sigma x \quad (A5)$$

Reducing Eq (5) to:

$$\ln \frac{I}{I_0} = -n\sigma x \quad (A6)$$

Substituting for $n\sigma x$ from Eq (A5):

$$\ln \frac{I}{I_0} = -9.658 \times 10^{18} \frac{P_{Cl_2}}{T_{Cl_2}} \sigma x \quad (A7)$$

Using the 3131\AA line and letting $x = 78$ cm (the length of the gas filled tube) Eq (A7) reduces to:

$$\frac{-T_{Cl_2}}{65.615} \ln \frac{I}{I_0} = P_{Cl_2} \quad (A8)$$

and using the σ for 3650\AA line, Eq (A7) reduces to:

$$\frac{-T_{Cl_2}}{35.167} \ln \frac{I}{I_0} = P_{Cl_2} \quad (A9)$$

Appendix B

This appendix presents the derivation of the standard deviation formula for error analysis of results. Since data is only presented that was taken with the use of the 3650Å line, the derivation will use Eq (63)

$$\frac{-T}{35.167} \ln \frac{I}{I_0} = P$$

The standard mathematical procedure for finding the standard deviation was used, i.e.,

$$S_p^2 = \sum_1^n \left(\frac{\partial P}{\partial X_n} S_{X_n} \right)^2 \quad (B1)$$

where

S_p^2 = Variance of P

S_{X_n} = Standard Deviation of the n variable

Using Eq (B1) on Eq (63) it is found:

$$S_p^2 = \left(\frac{-\ln \frac{I}{I_0}}{35.167} \right)^2 S_T^2 + \left(-\frac{T}{35.167} I^{-1} \right)^2 S_I^2 + \left(\frac{T}{35.167} I_0^{-1} \right)^2 S_{I_0}^2 \quad (B2)$$

The S_T was taken to equal 0.5°K and S_I and S_{I_0} were found from the data. Factoring out $(35.167)^{-2}$ and taking the square root of Eq (62), the formula used is found:

$$S_p = 0.0284357 \sqrt{(S_T \ln \frac{I}{I_0})^2 + (TS_I I^{-1})^2 + (TS_{I_0} I_0^{-1})^2} \quad (B3)$$

The error of the data points plotted used this formula and were refined before graphing (Ref 77).

Vita

Jerry D. Winegarden was born on 17 December 1956 in Gaylord, Michigan. He is the son of Mr and Mrs F. Dean Winegarden of Petoskey, Michigan. In June of 1975 he graduated from Petoskey High School, Petoskey, Michigan. He received a B.S. degree in Applied Physics from Michigan Technological University, Houghton, Michigan in 1979 and was commissioned through the ROTC program and entered the Air Force Institute of Technology in June 1979. He was married to his wife, Megan, on 15 March 1980.

Permanent Address: 1005 Hazelton Street
Petoskey, MI 49770

This thesis was typed by Mrs Anna L. Lloyd.

Unclassified

SECURITY CLASSIFICATION OF THIS PAGE (When Data Entered)

REPORT DOCUMENTATION PAGE		READ INSTRUCTIONS BEFORE COMPLETING FORM
1. REPORT NUMBER AFIT/GEP/PH/80-12	2. GOVT ACCESSION NO. AD-A094404	3. RECIPIENT'S CATALOG NUMBER
4. TITLE (and Subtitle) THE MEASUREMENT OF Cl_2 CONCENTRATION IN A $XeCl$ HOLLOW CATHODE DISCHARGE INCLUDING THE EFFECT OF H_2 ADDITION		5. TYPE OF REPORT & PERIOD COVERED MS Thesis
7. AUTHOR(s) Jerry D. Winegarden 2nd Lt USAF		6. PERFORMING ORG. REPORT NUMBER
9. PERFORMING ORGANIZATION NAME AND ADDRESS Air Force Institute of Technology (AFIT-EN) Wright-Patterson AFB, OH 45433		8. CONTRACT OR GRANT NUMBER(s)
11. CONTROLLING OFFICE NAME AND ADDRESS		10. PROGRAM ELEMENT, PROJECT, TASK AREA & WORK UNIT NUMBERS
14. MONITORING AGENCY NAME & ADDRESS (if different from Controlling Office)		12. REPORT DATE December 1980
		13. NUMBER OF PAGES 99
		15. SECURITY CLASS. (of this report) UNCLASSIFIED
		15a. DECLASSIFICATION/DOWNGRADING SCHEDULE
16. DISTRIBUTION STATEMENT (of this Report) Approved for public release; distribution unlimited.		
17. DISTRIBUTION STATEMENT (of the abstract entered in Block 20, if different from Report)		
18. SUPPLEMENTARY NOTES Approved for public release; IAW AFR 190-17 FREDERICK C. LYNCH, Major, USAF Director of Public Affairs 06 JAN 1981		
19. KEY WORDS (Continue on reverse side if necessary and identify by block number) Hollow Cathode Discharge $XeCl$ Excimer Photon Counting		
20. ABSTRACT (Continue on reverse side if necessary and identify by block number) A hollow cathode discharge tube was used to excite a $HCl/Xe/Ne$ gas mixture of 4%/16%/80%. Total gas pressures of 4 and 6 Torr and discharge currents ranging from 200, 300, 400, and 500 mA were investigated. A photon counting technique was used in a U.V. absorption spectroscopy experiment to determine the partial pressure of Cl_2 as a function of current and pressure and for monitoring the 308 nm emission of $XeCl$ for these conditions. $XeCl$ emission decreased with time as a result of the introduction of additional chlorine to the system from the discharge tube surface. Both this surface supplied chlorine and that		

DD FORM 1 JAN 73 1473 EDITION OF 1 NOV 65 IS OBSOLETE

UNCLASSIFIED

SECURITY CLASSIFICATION OF THIS PAGE (When Data Entered)

UNCLASSIFIED

SECURITY CLASSIFICATION OF THIS PAGE (When Data Entered)

originating from the HCl in the original mix resulted in a substantial concentration of Cl_2 being observed. The surface desorption rate increased with current and was dramatically enhanced by the addition of small amounts of H_2 to the discharge mix.

UNCLASSIFIED

SECURITY CLASSIFICATION OF THIS PAGE (When Data Entered)

NO
ATE